

CLASSIFICATION CHANGED
UNCLASSIFIEDTO NASA 4070629 10/30/70
By Library of Date 10/30/70TECHNICAL MEMORANDUM
X-285Declassified by authority of NASA
Classification Change Notices No. 211
Dated ** 12/31/70WIND-TUNNEL INVESTIGATION AT LOW SUBSONIC SPEEDS OF THE
STATIC AND OSCILLATORY STABILITY CHARACTERISTICS OF
MODELS OF SEVERAL SPACE CAPSULE CONFIGURATIONS

By Joseph L. Johnson, Jr.

Langley Research Center
Langley Field, Va.

FACILITY FORM 602

N71 - 70290

(ACCESSION NUMBER)

(THRU)

48
(PAGES)None
(CODE)

(NASA CR OR TMX OR AD NUMBER)

(CATEGORY)

NATIONAL AERONAUTICS AND SPACE ADMINISTRATION

WASHINGTON

May 1960

DECLASSIFIED

NATIONAL AERONAUTICS AND SPACE ADMINISTRATION

TECHNICAL MEMORANDUM X-285

WIND-TUNNEL INVESTIGATION AT LOW SUBSONIC SPEEDS OF THE
STATIC AND OSCILLATORY STABILITY CHARACTERISTICS OF
MODELS OF SEVERAL SPACE CAPSULE CONFIGURATIONS*

By Joseph L. Johnson, Jr.

SUMMARY

A wind-tunnel investigation at low subsonic speeds has been conducted in the Langley free-flight and full-scale tunnels to measure the static and oscillatory stability characteristics of models of several space capsule configurations. Included in the investigation were power-on tests to determine the effect of rocket-engine exhaust on the static stability characteristics of the NASA capsule model in the escape configuration.

The results indicated that the capsule models in the reentry configuration (blunt end forward) were statically stable at low angles of attack but had negative damping about the transverse axis. In the exit configuration (canister end forward) the capsule models were statically unstable over the angle-of-attack range of the tests but had positive damping about the transverse axis. In the escape configuration, the models had static stability (power-off condition) only at low angles of attack. From power-on tests of the escape configuration at conditions representing an abort prior to launch, it was found that the jet exhaust substantially increased the static stability at low angles of attack and increased the angle of attack at which instability occurred. The Little Joe booster-capsule configuration was statically stable and had positive damping over the angle-of-attack range investigated.

INTRODUCTION

The National Aeronautics and Space Administration is conducting a general research investigation to provide some basic information on blunt nonlifting reentry bodies at high and low speeds. In addition to

this basic research, a wind-tunnel program is also being conducted in direct support of Project Mercury for the NASA Space Task Group. As part of this work, tests were conducted in the Langley free-flight and full-scale tunnels to determine the low-subsonic static and oscillatory stability characteristics of several space capsule models.

The investigation included static and dynamic force tests of models of the NASA and McDonnell capsules in the exit, reentry, and escape configurations. Also tested were a model of the McDonnell capsule with a modified escape tower and a model of the Little Joe booster-capsule configuration. The effects of power on the static stability characteristics of the NASA capsule escape configuration were also determined in tests in which the rocket engine exhaust was simulated by compressed air jets. The investigation also included flow survey studies of the reentry configuration in order to obtain some visual observation of the nature of the flow in the vicinity of the model for use in correlation with the force test results.

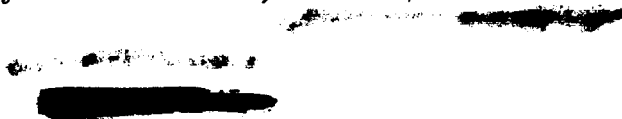
L
9
0
7

Since the capsule is a body of revolution, stability about a transverse axis may be called either longitudinal or directional stability. In this report it will be considered longitudinal stability; therefore, most of the data are presented as variations of pitching-moment, normal-force, and axial-force coefficients with angle of attack.

SYMBOLS

The data are referred to the body system of axes originating at the model center of gravity. The positive direction of forces, moments, and angular displacements is shown in figure 1.

S	maximum cross-sectional area perpendicular to X body axis, sq ft
d	maximum body diameter, ft
q_{∞}	free-stream dynamic pressure, lb/sq ft
α	angle of attack of model center line, deg
$\dot{\alpha}$	rate of change of angle of attack, radians/sec
V	free-stream velocity, ft/sec
ω	circular frequency of oscillation, radians/sec



DECLASSIFIED

3

k	reduced-frequency parameter, $\frac{\omega d}{2V}$
R	Reynolds number
q	pitching angular velocity, radians/sec
β	angle of sideslip, deg
\dot{q}	rate of change of pitching angular velocity, radians/sec
X,Z	longitudinal and vertical body axes, respectively
δ_n	nozzle extension angle, deg
C_A	axial-force coefficient, $\frac{\text{Axial force}}{q_\infty S}$
C_D	drag-force coefficient, $\frac{\text{Drag force}}{q_\infty S}$
C_N	normal-force coefficient, $\frac{\text{Normal force}}{q_\infty S}$
C_L	lift-force coefficient, $\frac{\text{Lift force}}{q_\infty S}$
C_T	thrust coefficient, $\frac{\text{Thrust}}{q_\infty S}$
C_m	pitching-moment coefficient, $\frac{\text{Pitching moment}}{q_\infty S d}$
C_Y	lateral-force coefficient, $\frac{\text{Lateral force}}{q_\infty S}$
C_n	yawing-moment coefficient, $\frac{\text{Yawing moment}}{q_\infty S d}$
C_l	rolling-moment coefficient, $\frac{\text{Rolling moment}}{q_\infty S d}$

03:30:00

$$C_{N\alpha} = \frac{\partial C_N}{\partial \alpha}, \text{ per deg}$$

$$C_{m\alpha} = \frac{\partial C_m}{\partial \alpha}, \text{ per deg}$$

$$C_{m\dot{q}} = \frac{\partial C_m}{\partial \frac{\dot{q}d}{2V}}$$

$$C_{N\dot{q}} = \frac{\partial C_N}{\partial \frac{\dot{q}d^2}{4V^2}}$$

$$C_{m\dot{q}} = \frac{\partial C_m}{\partial \frac{\dot{q}d^2}{4V^2}}$$

$$C_{m\ddot{\alpha}} = \frac{\partial C_m}{\partial \frac{\ddot{\alpha}d}{2V}}$$

L
9
0
7

APPARATUS AND MODELS

Most of the investigation was made with 1/4-scale models of the NASA and McDonnell capsules in the exit, reentry, and escape configurations. Also used in the investigation were a 0.30-scale model of the McDonnell capsule with a modified escape tower and a 1/10-scale model of the Little Joe booster-capsule configuration. Drawings of these models are presented in figure 2 and a photograph is presented in figure 3. The escape configuration of the NASA capsule was so constructed that compressed air could be exhausted through the rocket nozzles to provide thrust for power-on tests. (See fig. 2(c).) In this arrangement, compressed air was supplied to the model through a flexible hose which passed internally through the capsule and along the center line of the escape tower to the rocket motor. From the rocket motor, which served as a plenum chamber, the compressed air exhausted through converging-diverging nozzles to simulate the rocket engine exhaust. For a few tests, extensions were added to the basic nozzles to direct the jet exhaust from the design nozzle angle of 15° to other nozzle angles which varied from 0° to 30°.

03:30:00

The static force tests were conducted in the Langley free-flight and full-scale tunnels with sting-type support systems and strain-gage balances. A photograph of the free-flight tunnel static-force-test setup with the model of the NASA capsule in the escape configuration mounted for testing is shown in figure 4. The dynamic force tests were made in the free-flight tunnel using an oscillation apparatus which permitted the model to have freedom in pitch. Sketches of this apparatus with several different models mounted for pitching oscillation tests are shown in figure 5. In this apparatus, electrical resolvers were geared directly to the drive-shaft mechanism to generate electrical signals proportional to the displacement and velocity of the model. This resolver system permitted a direct reading of the balance output signals either in phase with or out of phase with angular displacement of the model by means of manually operated, null-seeking, readout equipment. A complete description of this apparatus and instrumentation is presented in reference 1.

TESTS

Static and dynamic force tests were made over an angle-of-attack range from 0° up to 180° to determine the static and oscillatory longitudinal stability characteristics of models of the NASA and McDonnell capsules in the exit, reentry, and escape configurations. In addition, a few tests were made to determine the effects of Reynolds number and the effects of modifications to the basic NASA capsule design (increased canister length and the addition of canister fins) on the stability characteristics of the model.

In addition to the power-off tests, the NASA capsule model in the escape configuration was tested over an angle-of-attack range from -40° to 40° with power on for a range of thrust coefficients from about 2.4 to about 10.0. The effects on stability of nozzle angle and of asymmetrical conditions in thrust and escape tower configuration were also investigated.

Flow survey studies were made in the Langley free-flight and full-scale tunnels of the reentry configuration with tufts attached to the surface of the model and to rods extending above and below the model and with a tuft grid at several stations back of the maximum diameter of the capsule.

The force tests and flow survey studies were made for a dynamic pressure range from about 1.4 to about 7.0 pounds per square foot which corresponds to a velocity range of about 34 feet per second to about 77 feet per second and to a Reynolds number range from about 0.32×10^6

031320 1030

to about 0.80×10^6 based on the maximum diameter of the models investigated. The dynamic force tests were made for amplitudes in pitch of $\pm 5^\circ$ and for a frequency range from 0.25 to 1.00 cycle per second which corresponds to a range of the reduced-frequency parameter k of about 0.02 to 0.07.

RESULTS AND DISCUSSION

Presentation of Data

Data for the capsule models in the exit and reentry configurations are shown in figures 6 to 14. Data for the capsule models in the escape configuration are shown in figures 15 to 23. Data for the Little Joe booster-capsule configuration are shown in figures 24 and 25. An index to the data is presented in table I.

Exit and Reentry Configurations

Static longitudinal stability characteristics.— The longitudinal data for the McDonnell capsule model are presented in figure 6(a) for an angle-of-attack range from 0° to 180° and for a Reynolds number range from 0.34×10^6 to 0.70×10^6 . The data show that the McDonnell capsule model was statically longitudinally stable in the reentry configuration (blunt end forward) but was unstable in the exit configuration (canister end forward). The stability of the reentry configuration decreased above an angle of attack of 30° , but the model had a restoring moment through the angle-of-attack range of the tests. In the region of an angle of attack of 90° this restoring moment was appreciably reduced. The reentry configuration had a negative slope of the normal-force curve at low angles of attack which is characteristic of blunt, sharp-edge bodies of this type.

The lift and drag data for the model (fig. 6(b)) show a negative slope of the lift curve at low angles of attack and negative values of lift coefficient through an angle of attack of about 90° .

A comparison plot of the static longitudinal stability data obtained for the McDonnell and NASA capsule models is presented in figure 7. These data show no great difference in the characteristics of the two models.

The data from tests made to determine the effect on the longitudinal stability characteristics of the NASA capsule model of increasing the canister length and of adding fins to the canister are presented in figure 8. These data show that, as expected, increasing the canister length

L
9
0
7

DECLASSIFIED

7

or adding fins to the canister increased the static longitudinal stability, reduced the negative slope of the normal-force curve at low angles of attack, and increased the normal-force coefficient at high angles of attack.

Presented in figures 9(a) and 9(b) are longitudinal data for the NASA capsule model obtained in the present investigation compared with data obtained from full-size model tests at low speeds in the Langley full-scale tunnel (data taken from ref. 2). These data show that increasing the Reynolds number from less than 1×10^6 to 4.85×10^6 decreased the static stability somewhat but generally did not greatly affect the other characteristics of the configuration.

Static lateral characteristics.- Force tests were made to determine the lateral forces and moments of the McDonnell capsule model in the reentry configuration at 0° sideslip for an angle-of-attack range from 0° to 90° . The results of these tests are presented in figure 10 and show relatively large yawing moments for angles of attack of about 40° to 90° . A plot of C_n/C_m against α indicates that at some of the higher angles of attack the yawing moments were equal to or greater than the pitching moments. These results appear to explain unpublished results obtained in the Langley spin-tunnel dynamic tests of this reentry configuration. In these tests the capsule usually oscillated in one plane at about a constant amplitude up to angles as high as 90° , but at times the model stopped this type of motion at the peak of an oscillation and started rotating about the vertical wind axis, apparently because of some lateral disturbance.

Flow studies of reentry configuration.- In order to obtain some visual observation of the nature of the flow around the capsule model in the reentry configuration, flow surveys were made with tufts attached to the surface of the model and to rods extending above and below the model. Photographs of the model in this setup are shown in figure 11 for an angle-of-attack range from 0° to 40° . At an angle of attack of 0° these photographs show a region of disturbed flow behind the model which extended beyond the maximum diameter of the blunt surface. Within this disturbed flow region the air flow is generally opposite in direction to that of the free stream. This reversed flow almost completely immersed all of the model back of the blunt forward surface. At high angles of attack, the photographs show that the disturbed flow region was above the model and that smooth air flow swept the lower surface of the model in an upward direction.

In addition to the flow studies made to determine the nature of the flow around the model, tuft grid and flow survey measurements were made at several stations back of the reentry configuration. The results of these flow survey measurements are presented in figure 12 in the form of

03170291030

contours of constant lines of q/q_∞ (ratio of local dynamic pressure to free-stream dynamic pressure) and downwash- and sidewash-angle vectors denoting deviations from the free-stream direction. Although the results of the flow measurements are presented as constant values of q/q_∞ and angular deviations, actually these measurements were changing continually at each station because of the random nature of the flow around the capsule. The values of q/q_∞ and the angular deviations plotted in figure 12 are therefore average measurements taken over a considerable length of time. These data show that at 9 diameters back of the model (fig. 12(a)) there was a maximum loss in dynamic pressure of about 25 percent and maximum deviations in air flow of the order of 3° or 4° . This station is the approximate location of the main parachute canopy for the landing phase of the capsule flight program. The flow measurements at 6 and 3 diameters back of the capsule (figs. 12(b) and 12(c)) show maximum losses in dynamic pressure of about 35 percent and 67 percent, respectively, and considerably higher deviation of air flow than at the 9-diameter station.

Pitching oscillation derivatives.- The pitching oscillation derivatives measured at several different values of the reduced-frequency parameter k are presented in figures 13 and 14 for the McDonnell and NASA capsule models, respectively. The data of figure 13 show that the McDonnell capsule had negative damping in pitch ($C_{m_q} + C_{m_{\dot{\alpha}}}$) in the reentry configuration and positive damping $-(C_{m_q} + C_{m_{\dot{\alpha}}})$ in the exit configuration. Above an angle of attack of about 30° the model generally had positive damping in pitch and, although the data show considerable scatter, there appears to be no consistent effect of frequency on the damping-in-pitch derivative. The derivatives measured in phase with displacement during the oscillation tests, $C_{N_\alpha} + k^2 C_{N_{\dot{\alpha}}}$ and $C_{m_\alpha} + k^2 C_{m_{\dot{\alpha}}}$, show no consistent effect of frequency and are in generally good agreement with the results of the static force tests ($k = 0$).

The pitching oscillation derivatives of the NASA capsule model in the reentry configuration (fig. 14) were measured at an angle of attack of 0° for the basic configuration and for the model with increased canister length and with fins added to the canister. These data show that the basic configuration had about the same amount of negative damping as the McDonnell capsule at $\alpha = 0^\circ$ and that increasing the canister length or adding canister fins made the model more undamped despite the fact that these configuration changes increased the static stability of the model. The data also show generally good agreement between the derivatives measured in phase with displacement during the oscillation tests and the results of static force tests.

SECRET

Although the data of figure 14 show much larger values of negative damping for the model with increased canister length than for the basic configuration, unpublished Langley spin-tunnel results have shown that the amplitude of the free-flight oscillations of the model with the increased length was only about $\pm 30^\circ$ whereas for the basic configuration this amplitude varied from $\pm 60^\circ$ to $\pm 90^\circ$. This result indicates that data measured at small amplitudes (such as that presented in the present investigation) may not be applicable in cases where the amplitudes of the oscillations are very large.

L
9
0
7
In order to obtain some information which might be useful in explaining the damping results of the reentry configuration, tufts were attached to the surface of the model (in a similar manner to that used in the flow studies of the static setup) and observed while the model was oscillating in pitch. Analysis of movies made of these studies showed that, as the model oscillated, the flow over the rear portion of the model was in the same direction as the motion of the rear portion of the model and therefore was in the direction to produce negative damping. This flow variation might be explained as follows: In the static condition, as pointed out earlier, increasing the angle of attack of the capsule produced an upwash over the rear portion of the capsule. This upwash tends to produce a statically stabilizing effect in much the same manner that the downwash behind a wing produces a statically destabilizing effect on the horizontal tail. For the dynamic case involving an oscillation in pitch, there is a lag in this upwash over the rear portion of the capsule which produces a decrease in damping in the same manner that the lag of downwash behind a wing increases the damping contributed by a horizontal tail. The destabilizing effect of the lag of upwash resulted in negative damping for angles of attack less than 30° . (See fig. 13.)

Escape Configuration

Presented in figure 15 are the data obtained with the McDonnell configuration at Reynolds numbers of 0.60×10^6 and 0.85×10^6 . These data show that the model had static stability only at low angles of attack.

A comparison of the data for the NASA configuration, the McDonnell configuration, and the McDonnell configuration with a modified escape tower (fig. 16) show generally similar trends in the static characteristics for the three configurations investigated. The McDonnell configuration with the modified escape tower showed much larger unstable pitching moments at the higher angles of attack.

SECRET

[REDACTED]

[REDACTED]

[REDACTED]

[REDACTED]

appear that the aerodynamic characteristics of the model would be primarily influenced by the exhaust from the forward rather than from the rearward side of the model.

Results of force tests in which the model was tested with just the two top nozzles exhausting or with just the lower nozzle exhausting (presented in fig. 19) tended to verify these observations that the aerodynamic characteristics of the model are primarily influenced by the exhaust from the forward nozzle. That is, the data show that the pitching moments for the basic three-nozzle configuration were more similar to those for the one-nozzle configuration at positive angles of attack and more similar to those for the two-nozzle configuration at negative angles of attack.

Presented in figure 20 are the results of studies of the effects of the jet exhaust on the aerodynamic characteristics of the model in which the angle of attack was varied in a plane 90° to that used in the previous tests. An angle-of-attack variation in this manner should result in symmetrical jet exhaust flow conditions over the model at positive and negative angles of attack. Force test data obtained for this condition show in fact that the data for this case are more nearly symmetrical at negative and positive angles of attack than the data of figure 18.

The results of tests to determine the effect of nozzle angle on the longitudinal characteristics of the model are presented in figure 21. The value of C_T of 10.20 is based on the thrust measured for the 15° nozzle angle condition and is used as a reference for the other angles since all the tests were made at the same line pressure. It is realized that this value of C_T is only approximate at the lower and and higher nozzle angles since the thrust was reduced slightly by the exhaust deflectors (see fig. 2(c)) and since the value of C_T measured along the X body axis varied as the cosine function of the nozzle angle. This reference value of C_T , however, represents an average thrust coefficient for the conditions investigated and is believed to be sufficiently accurate for determining qualitative effects of nozzle angle on the longitudinal stability characteristics of the model.

The data of figure 21 show large variations in the pitching-moment coefficient with nozzle angle. The 15° nozzle angle produced large favorable effects of the jet exhaust on the stability characteristics of the model and appeared to be the optimum nozzle angle from this standpoint for the range of nozzle angles tested. The $7\frac{1}{2}^\circ$ nozzle angle produced large destabilizing effects of the jet exhaust while the $22\frac{1}{2}^\circ$



and 30° nozzle angle conditions produced relatively small destabilizing effects. The 0° and $7\frac{1}{2}^\circ$ nozzle angle conditions are of little practical importance since in these cases the jet exhaust impinged directly on the front end of the canister. These results do indicate, however, that in cases where this type of impingement occurs there exists the possibility of instability. A plot of C_{m_α} against nozzle angle (determined for angles of attack of $\pm 5^\circ$ in fig. 21) is presented in figure 22 to show the effect of nozzle angle on the static stability parameter more clearly.

Pitching oscillation derivatives.— The pitching oscillation derivatives measured for the escape configuration of the McDonnell capsule are presented in figure 23 for values of k of 0.035 and 0.070. These data show that the model had positive damping in pitch $-(C_{m_q} + C_{m_{\dot{\alpha}}})$ at an angle of attack of 0° and that the damping increased as the angle of attack increased. Very little or no effect of frequency is shown by the data and the derivatives in phase with displacement are in good agreement with the static-force-test results ($k = 0$).

L
9
0
7

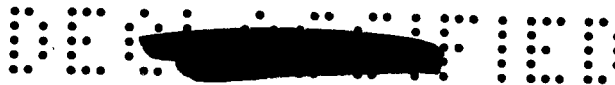
Capsule-Booster Configuration

Static longitudinal stability characteristics.— The static longitudinal stability characteristics of the Little Joe booster-capsule configuration are presented in figure 24. These data show that the configuration was statically longitudinally stable in the low angle-of-attack range and had an increase in restoring moment with increasing angle of attack up to 90° .

Pitching oscillation derivatives.— The pitching oscillation derivatives measured for the Little Joe booster-capsule configuration are presented in figure 25 for a value of k of 0.028. These data show that the configuration had positive damping in pitch at an angle of attack of 0° and that the damping generally increased up through an angle of attack of 70° . The derivatives measured in phase with displacement are in good agreement with the results of static tests.

The coefficients and derivatives presented in figures 24 and 25 for the capsule-booster configuration are very large in magnitude compared with those of the other capsule configurations tested because they were based on the maximum diameter and corresponding cross-sectional area of the booster rather than on the fin or tail area and tail span.





SUMMARY OF RESULTS

Results of wind-tunnel tests at low subsonic speeds to determine the static and oscillatory longitudinal stability characteristics of models of several space capsule configurations are summarized as follows:

1. The capsule models in the reentry configuration (blunt end forward) were statically longitudinally stable at low angles of attack but had negative damping in pitch. In the exit configuration (canister end forward) the capsule models were statically longitudinally unstable over the angle-of-attack range of the tests but had positive damping in pitch.

2. The capsule models in the escape configuration had static longitudinal stability (power-off condition) only at low angles of attack. From power-on tests of the escape configuration at conditions representing an abort prior to launch, it was found that the jet exhaust substantially increased the static stability at low angles of attack and increased the angle of attack at which instability occurred.

3. The Little Joe booster-capsule configuration was statically longitudinally stable and had positive damping in pitch over the angle-of-attack range investigated.

Langley Research Center,
National Aeronautics and Space Administration,
Langley Field, Va., February 18, 1960.

REFERENCES

1. Hewes, Donald E.: Low-Subsonic Measurements of the Static and Oscillatory Lateral Stability Derivatives of a Sweptback-Wing Airplane Configuration at Angles of Attack From -10° to 90° . NASA MEMO 5-20-59L, 1959.
2. Scallion, William I.: Full-Scale Wind-Tunnel Investigation of the Low-Speed Static Aerodynamic Characteristics of a Model of a Reentry Capsule. NASA TM X-220, 1959.





TABLE I

INDEX TO DATA

Capsule identification	Type of test	Angle-of-attack range	Plot of -	Figure
Exit and reentry configurations				
McDonnell	Static, longitudinal	0° to 180°	C_N , C_A , and C_m against α	6(a)
McDonnell	Static, longitudinal	0° to 90°	C_N , C_A , C_L , C_D , and C_m against α	6(b)
McDonnell and NASA	Static, longitudinal	0° to 90°	C_N , C_A , and C_m against α	7
NASA	Static, longitudinal	0° to 90°	C_N , C_A , and C_m against α	8
NASA	Static, longitudinal	0° to 90°	C_N , C_A , and C_m against α	9
McDonnell	Static, lateral	0° to 90°	C_Y , C_N , and C_l against α	10
McDonnell	Tuft flow studies	0° to 40°	Photographs	11
McDonnell	Tuft grid studies	0°	Downwash and sidewash angles, q/q_∞	12
McDonnell	Pitching oscillation	0° to 180°	$C_{N\alpha} + k^2 C_{N\dot{q}}$, $C_{m\alpha} + k^2 C_{m\dot{q}}$, $C_{mq} + C_{m\dot{q}}$ against α	13
NASA	Pitching oscillation	0°	$C_{N\alpha} + k^2 C_{N\dot{q}}$, $C_{m\alpha} + k^2 C_{m\dot{q}}$, $C_{mq} + C_{m\dot{q}}$ against α	14
Escape configuration				
McDonnell	Static, longitudinal	0° to 90°	C_N , C_A , and C_m against α	15
McDonnell and NASA	Static, longitudinal	0° to 180°	C_N , C_A , and C_m against α	16
McDonnell	Static, longitudinal	0° to 40°	C_N , C_A , and C_m against α	17
NASA	Static, longitudinal (power on)	-40° to 40°	C_N , C_A , and C_m against α for $C_T = 0, 2.4, 4.8$, and 9.9	18
NASA	Static, longitudinal (power on)	-40° to 40°	C_N , C_A , and C_m against α for $C_T = 3.27, 6.45$, and 10.20	19
NASA	Static, longitudinal	-40° to 40°	C_N , C_A , and C_m against α for $C_T = 2.38, 4.82$, and 9.9	20
NASA	Static, longitudinal	-40° to 40°	C_N , C_A , and C_m against α for nozzle angles of 0°, 7.5°, 15°, 22.5°, and 30°; $C_T = 10.20$	21
NASA	Static, longitudinal	-5° to 5°	$C_{m\alpha}$ against nozzle angle	22
McDonnell	Pitching oscillation	0° to 50°	$C_{N\alpha} + k^2 C_{N\dot{q}}$, $C_{m\alpha} + k^2 C_{m\dot{q}}$, $C_{mq} + C_{m\dot{q}}$ against α	23
Little Joe booster-capsule configuration				
McDonnell	Static, longitudinal	0° to 90°	C_N , C_A , and C_m against α	24
McDonnell	Pitching oscillation	0° to 90°	$C_{N\alpha} + k^2 C_{N\dot{q}}$, $C_{m\alpha} + k^2 C_{m\dot{q}}$, $C_{mq} + C_{m\dot{q}}$ against α	25

DECLASSIFIED

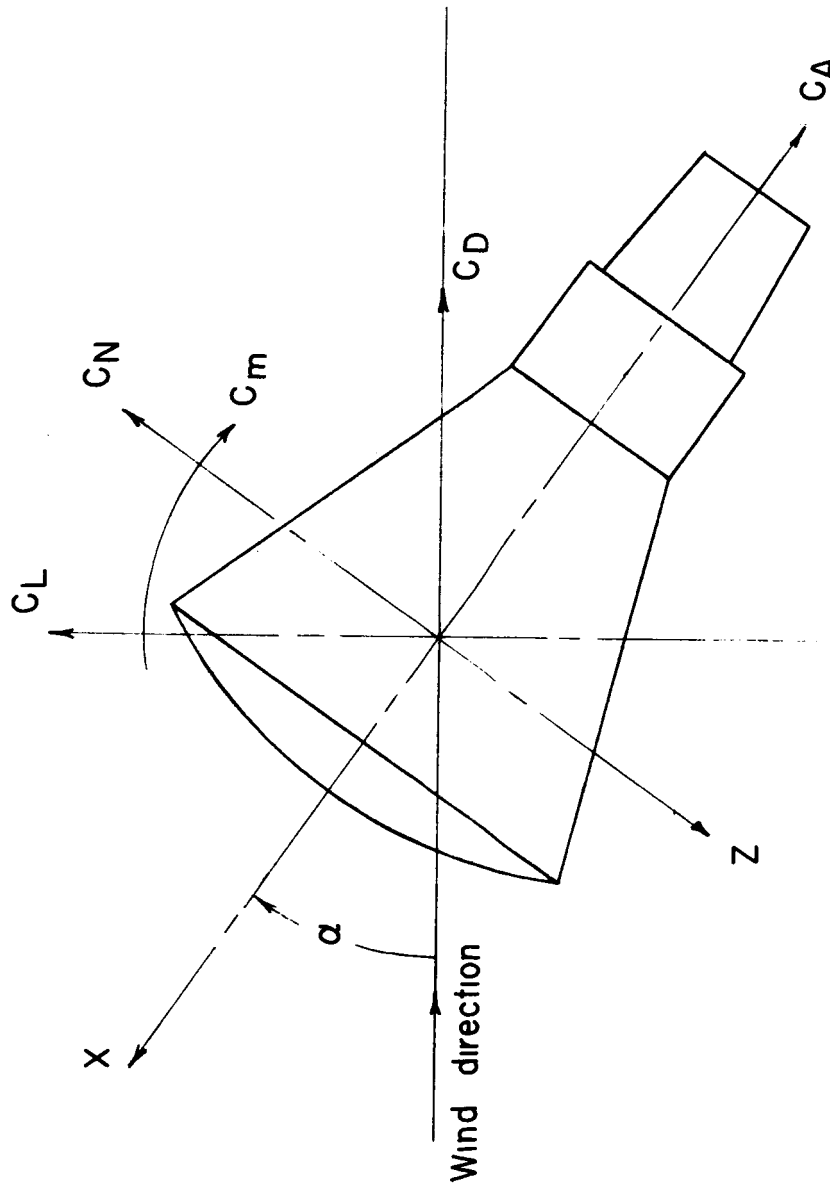
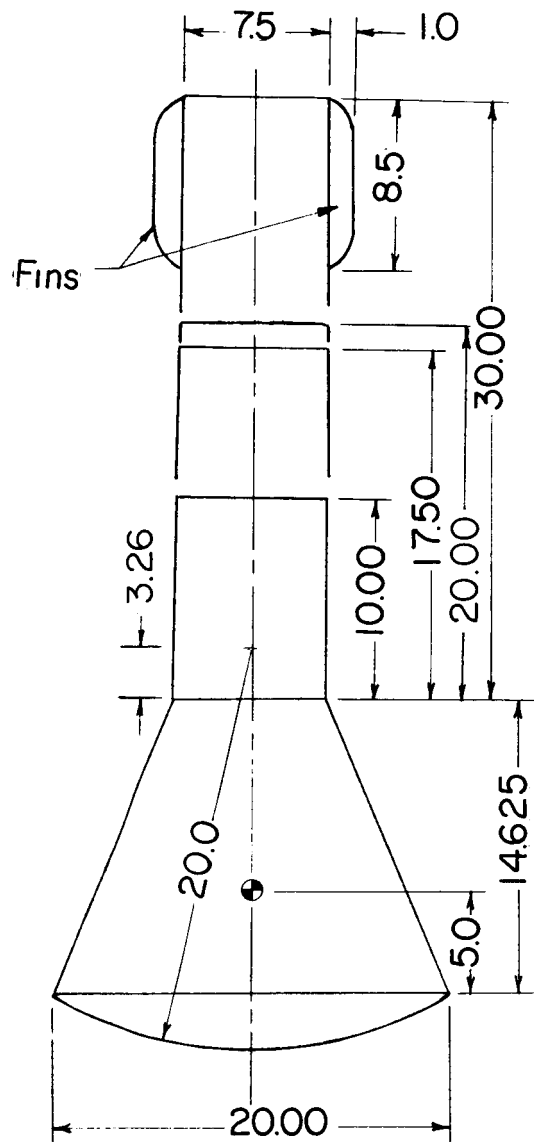
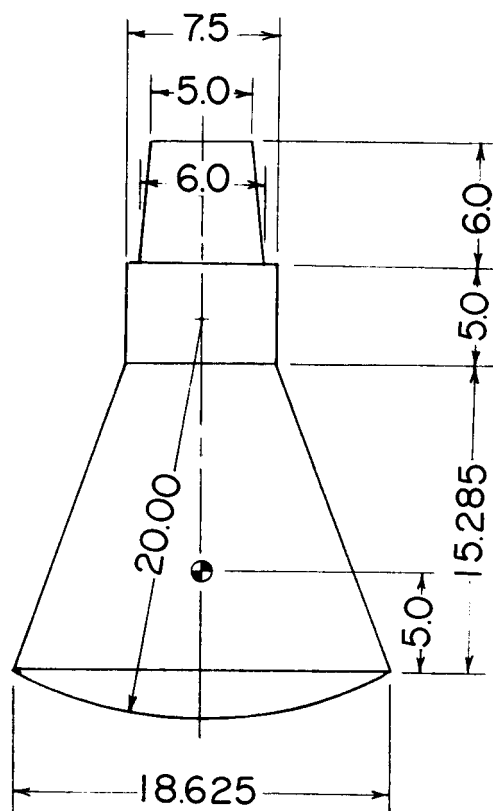


Figure 1.- System of axes used in the investigation. Arrows indicate positive directions.



NASA configuration

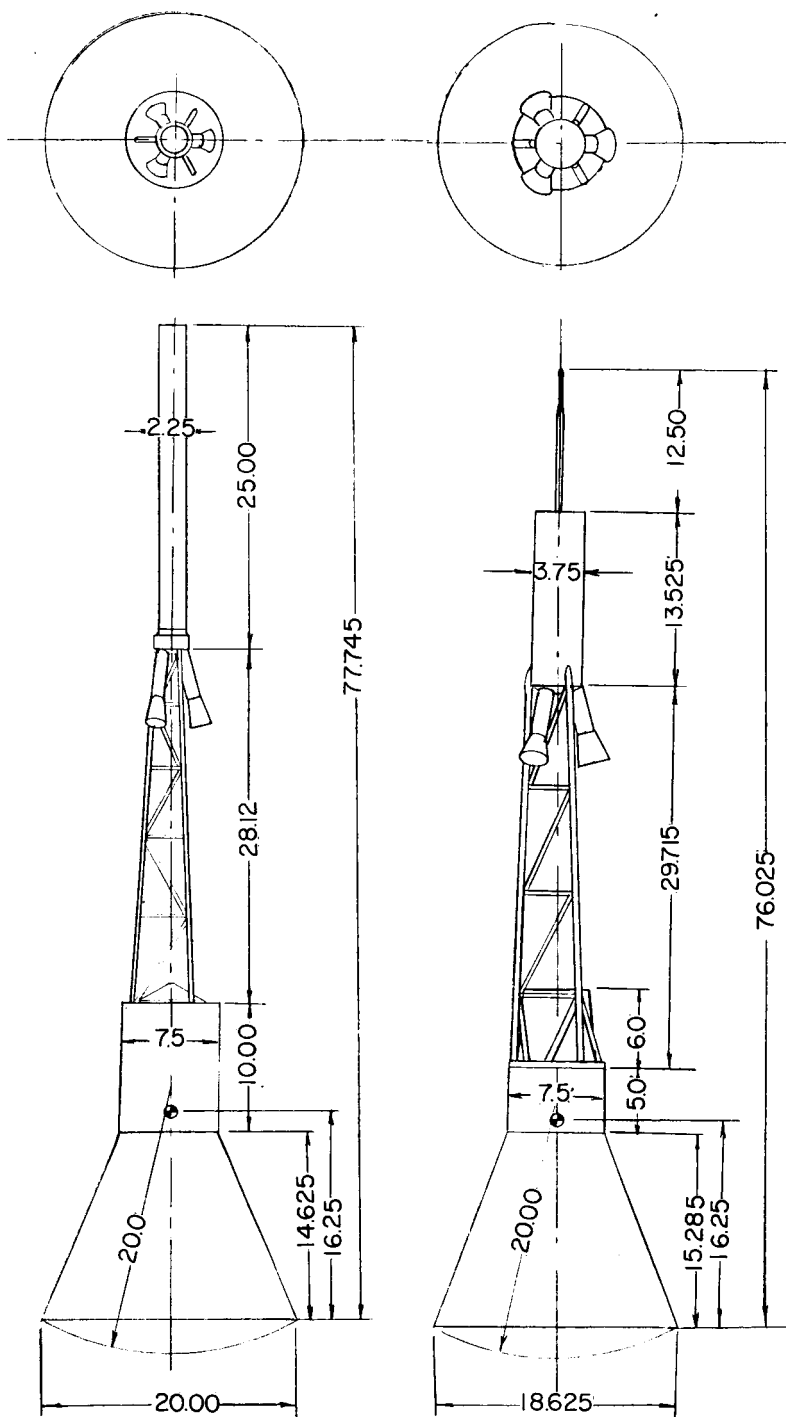


McDonnell configuration

(a) 1/4-scale models of the reentry and exit configurations.

Figure 2.- Sketches of models used in the investigation. All dimensions are in inches.

SECRET



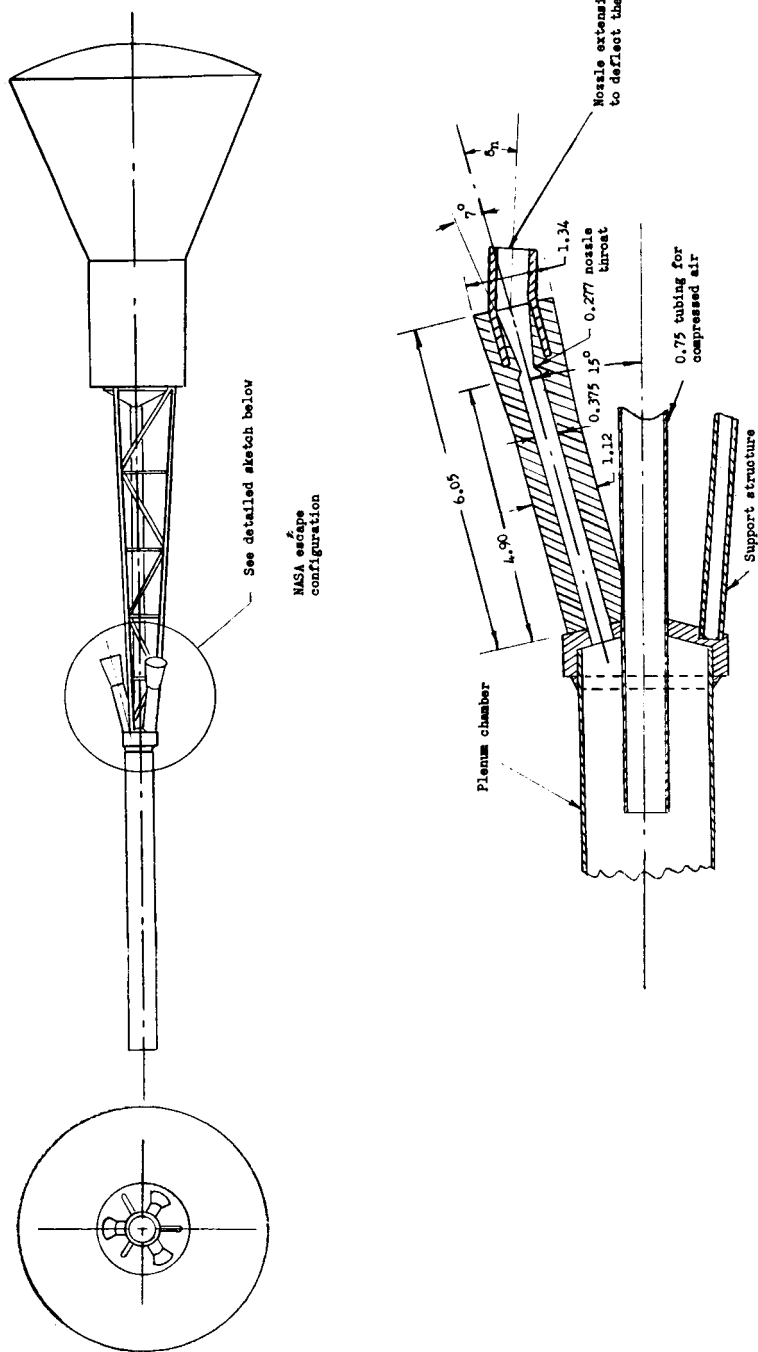
1/4-scale NASA model

1/4-scale McDonnell model

(b) Escape configurations.

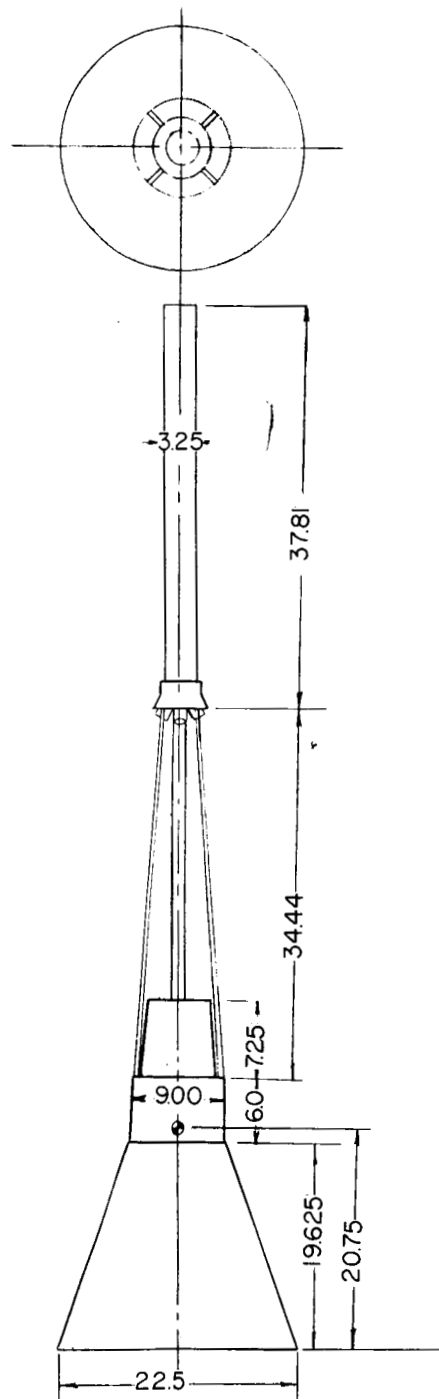
Figure 2.- Continued.

SECRET



(c) Section view of plenum chamber and nozzle assembly used in power-on tests with the model of the NASA escape configuration.

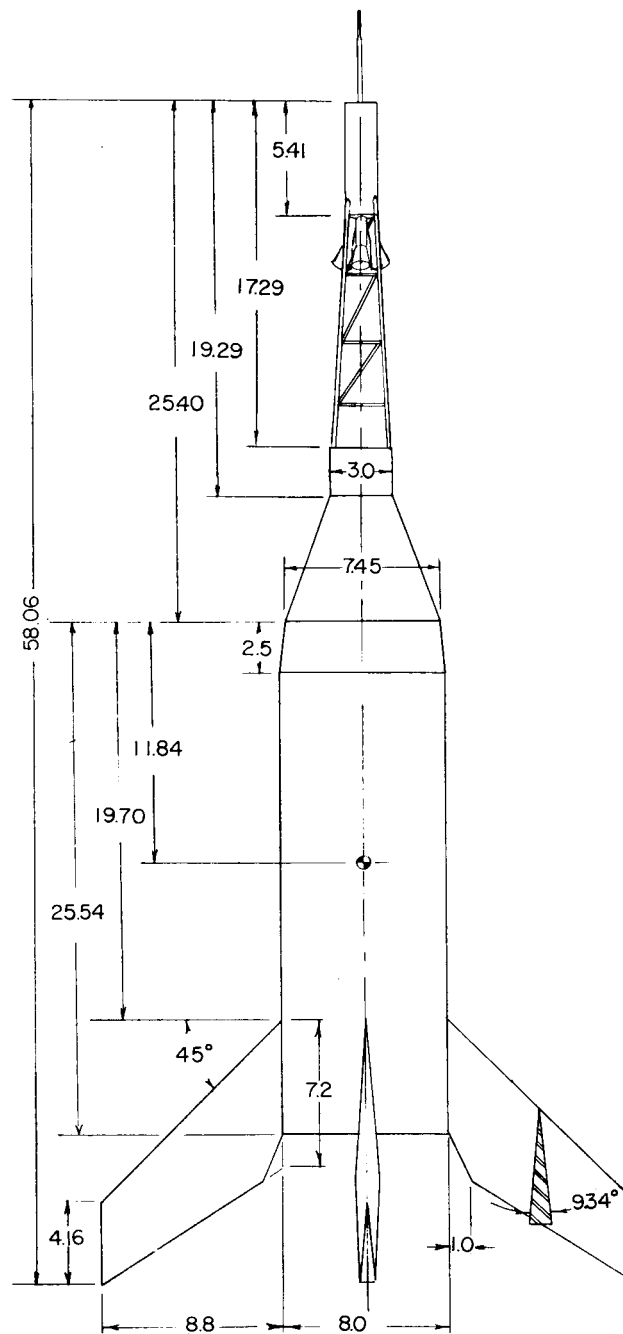
Figure 2.- Continued.



(d) 0.3-scale McDonnell model with modified escape tower.

Figure 2.- Continued.

037: [REDACTED] 030



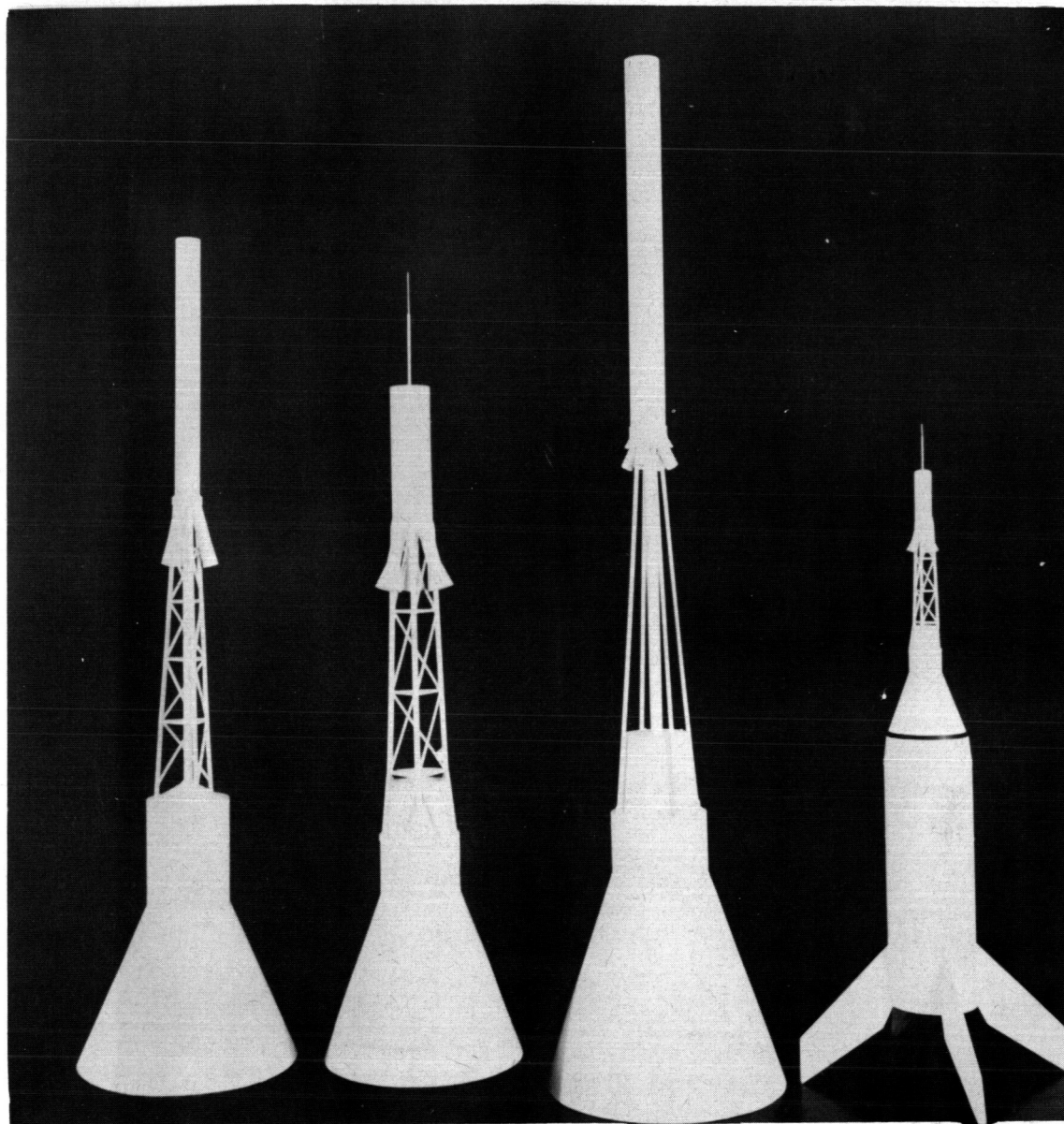
(e) Sketch of 1/10-scale model of the Little Joe booster-capsule configuration used in the investigation.

Figure 2.- Concluded.

[REDACTED]

~~CONFIDENTIAL~~

21



1/4-scale model
of NASA escape
configuration

1/4-scale model
of McDonnell
escape
configuration

3/10-scale model of
McDonnell escape
configuration with
modified tower

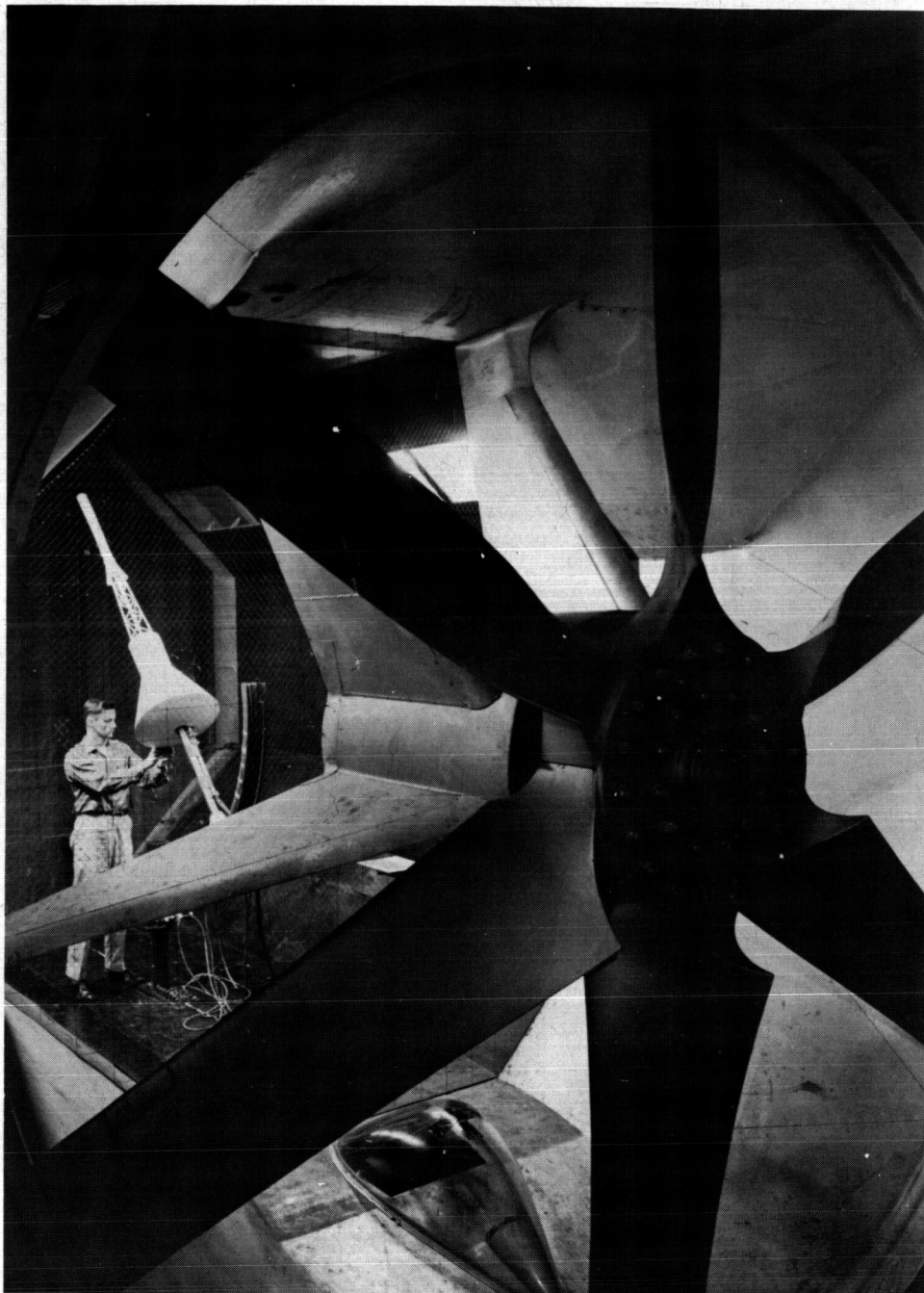
1/10-scale model
of Little Joe
booster-capsule
configuration

L-59-4683.1

Figure 3.- Photograph of models used in the investigation.

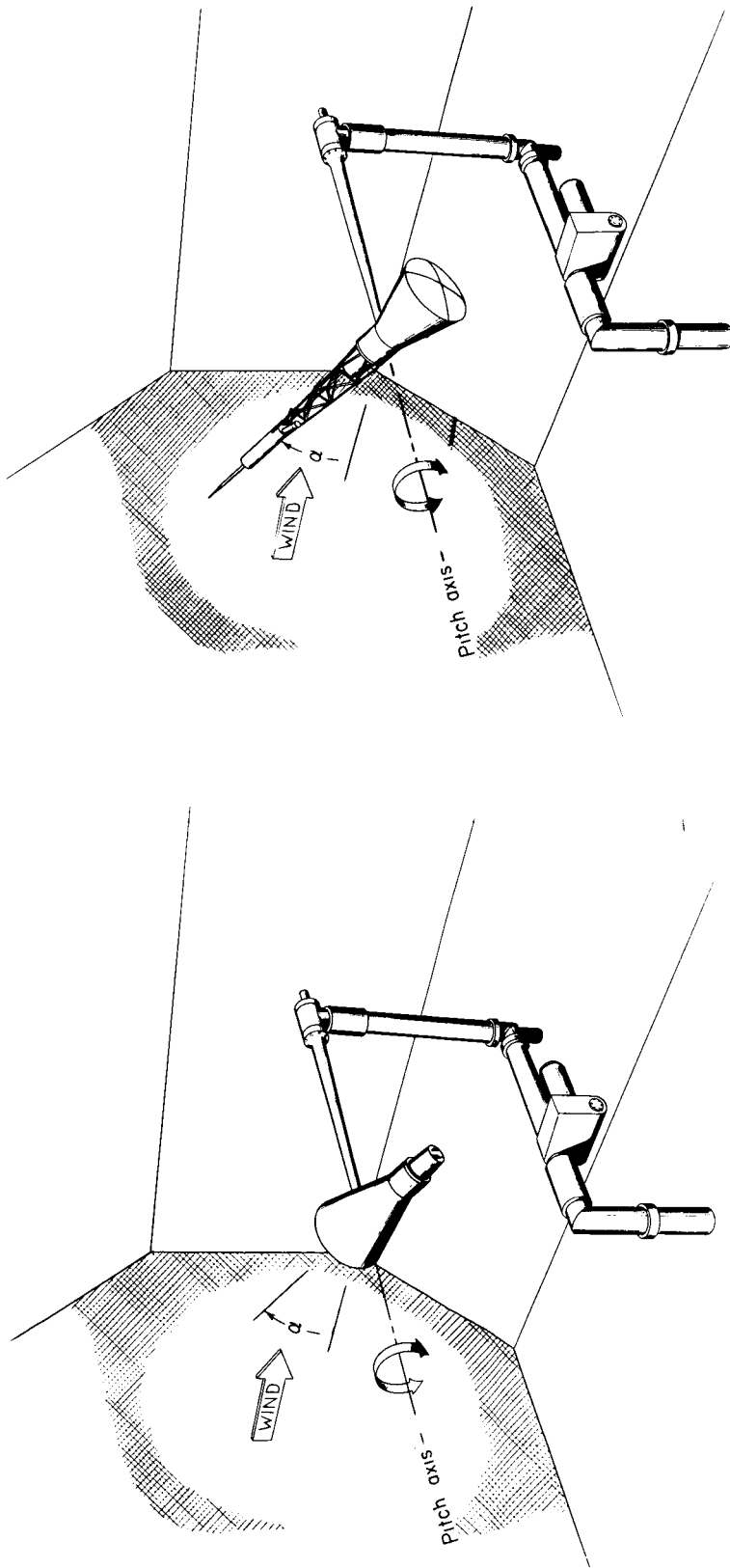
~~CONFIDENTIAL~~

CONFIDENTIAL



L-59-3177

Figure 4.- Photograph of the force test setup in the Langley free-flight tunnel with the 1/4-scale model of the NASA capsule model in the escape configuration mounted for testing.

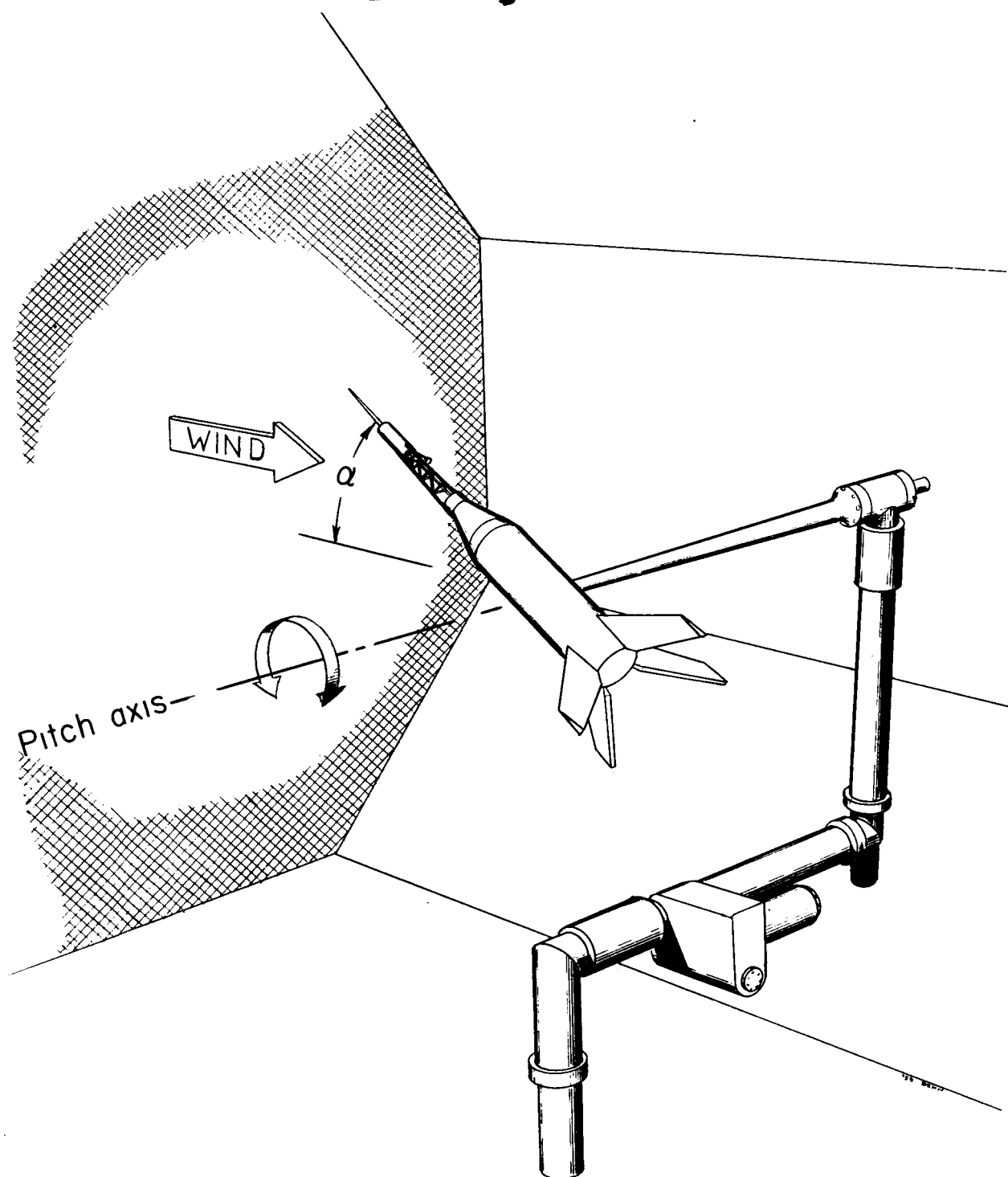


(a) Reentry configuration.

(b) Escape configuration.

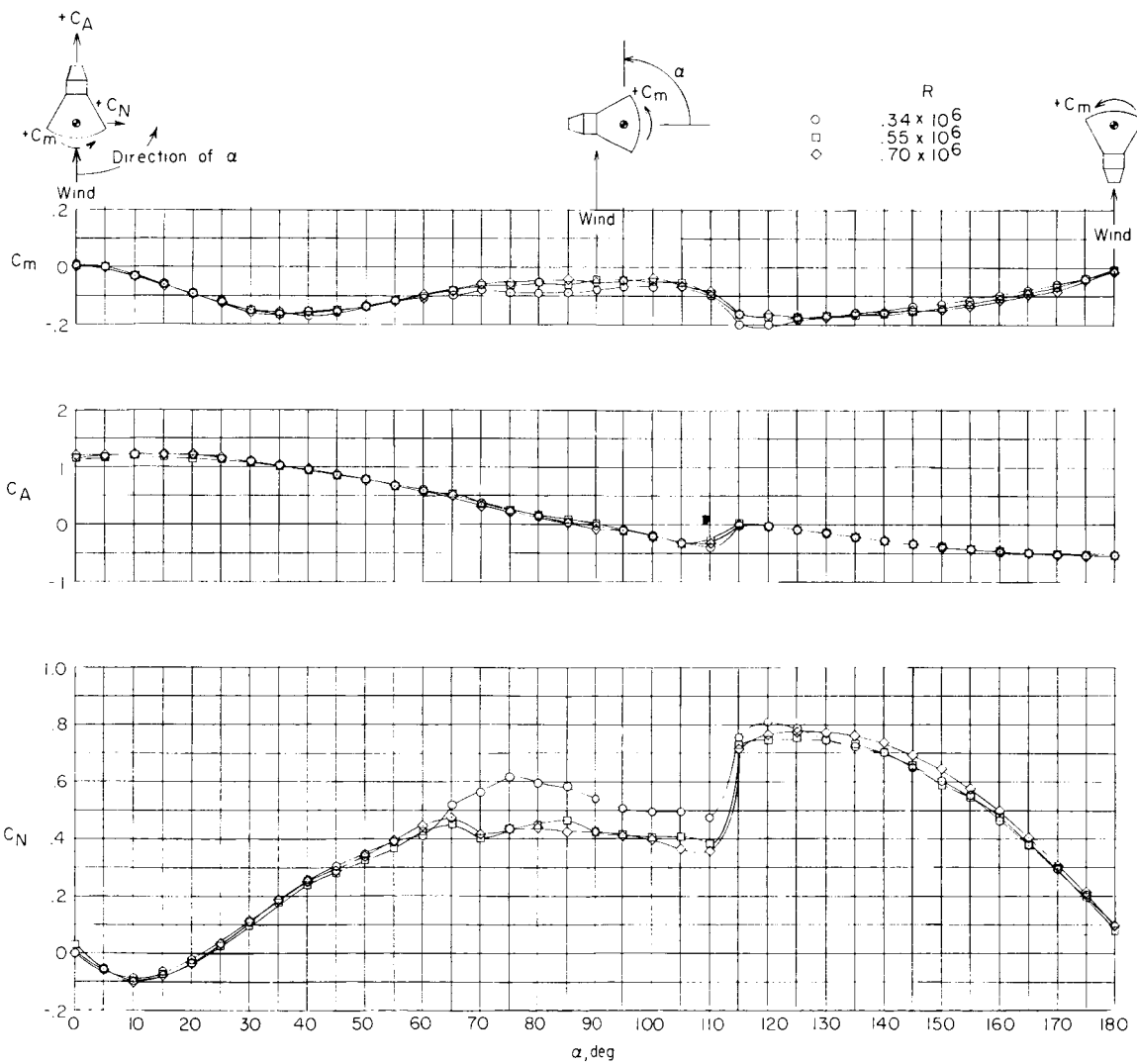
Figure 5.- Schematic sketches of models mounted for rotary oscillation tests in pitch.

03174241030



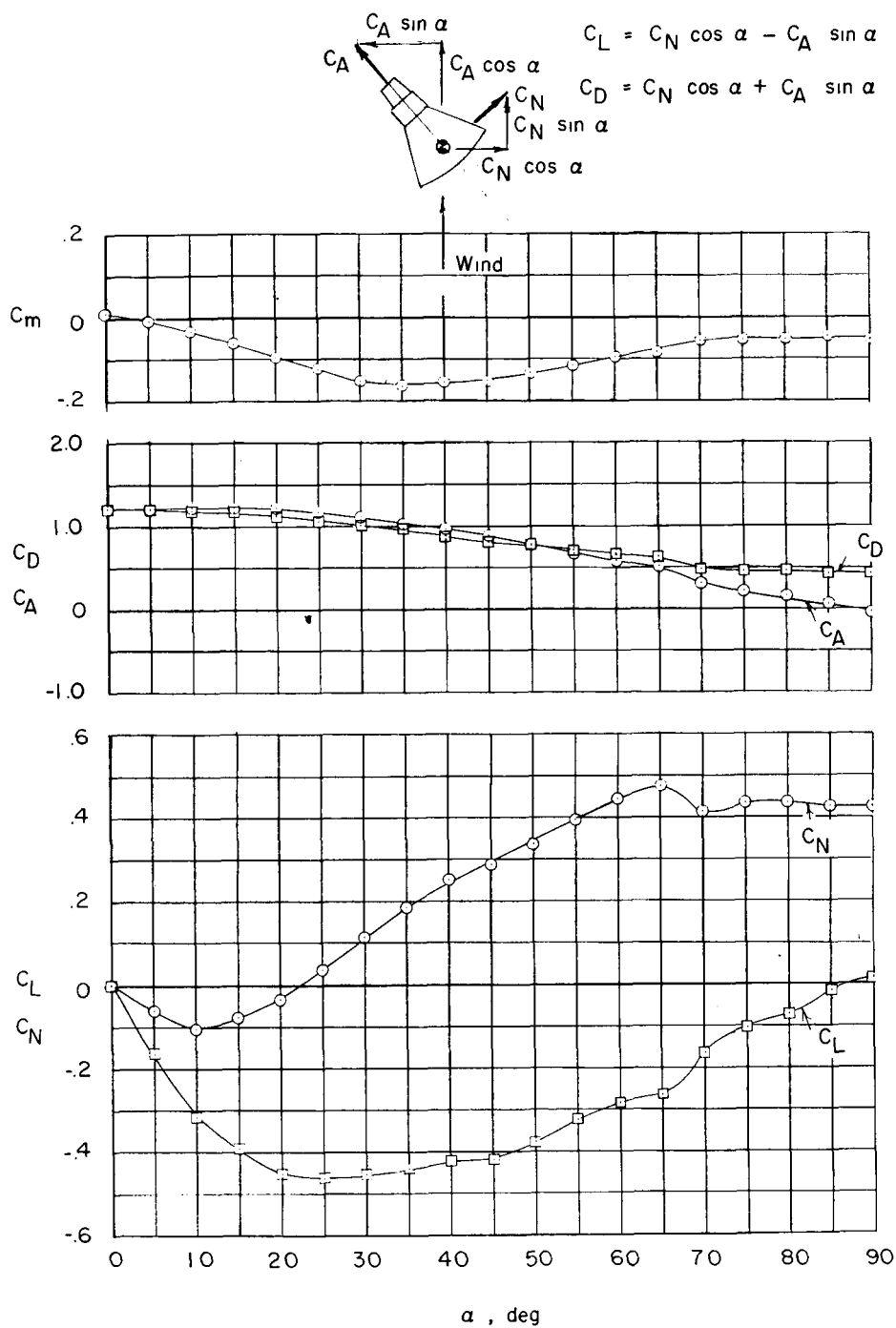
(c) Little Joe booster-capsule configuration.

Figure 5.- Concluded.



(a) Variation of C_m , C_A , and C_N with angle of attack for the reentry and exit configurations.

Figure 6.- Static longitudinal characteristics of the McDonnell capsule model.



(b) Comparison of longitudinal wind-axes data with body-axes data.

Figure 6.- Concluded.

[REDACTED]

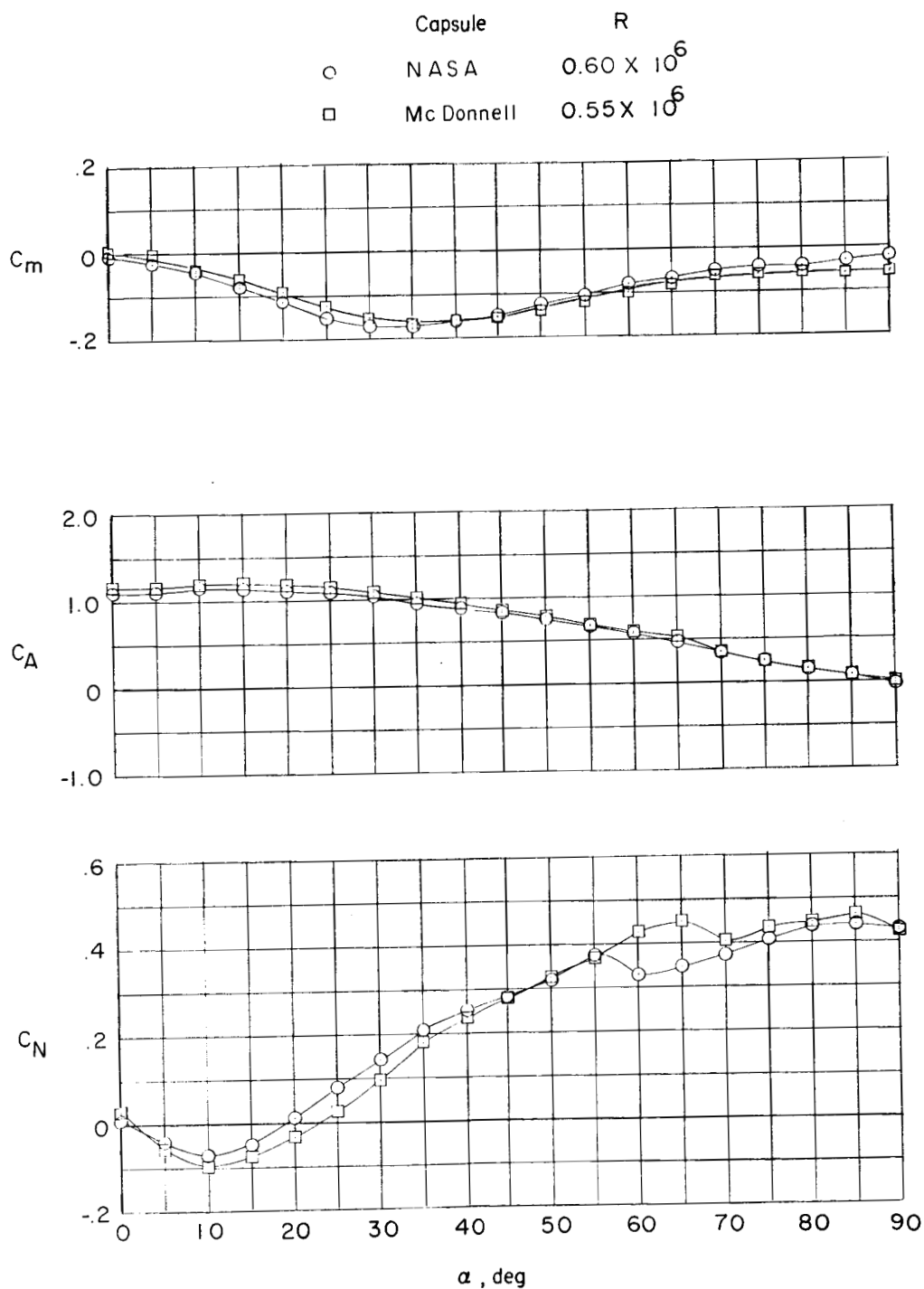


Figure 7.- Comparison of static longitudinal characteristics of the NASA and Mc Donnell capsule models in the reentry configuration.

[REDACTED]

0371 [REDACTED] 34

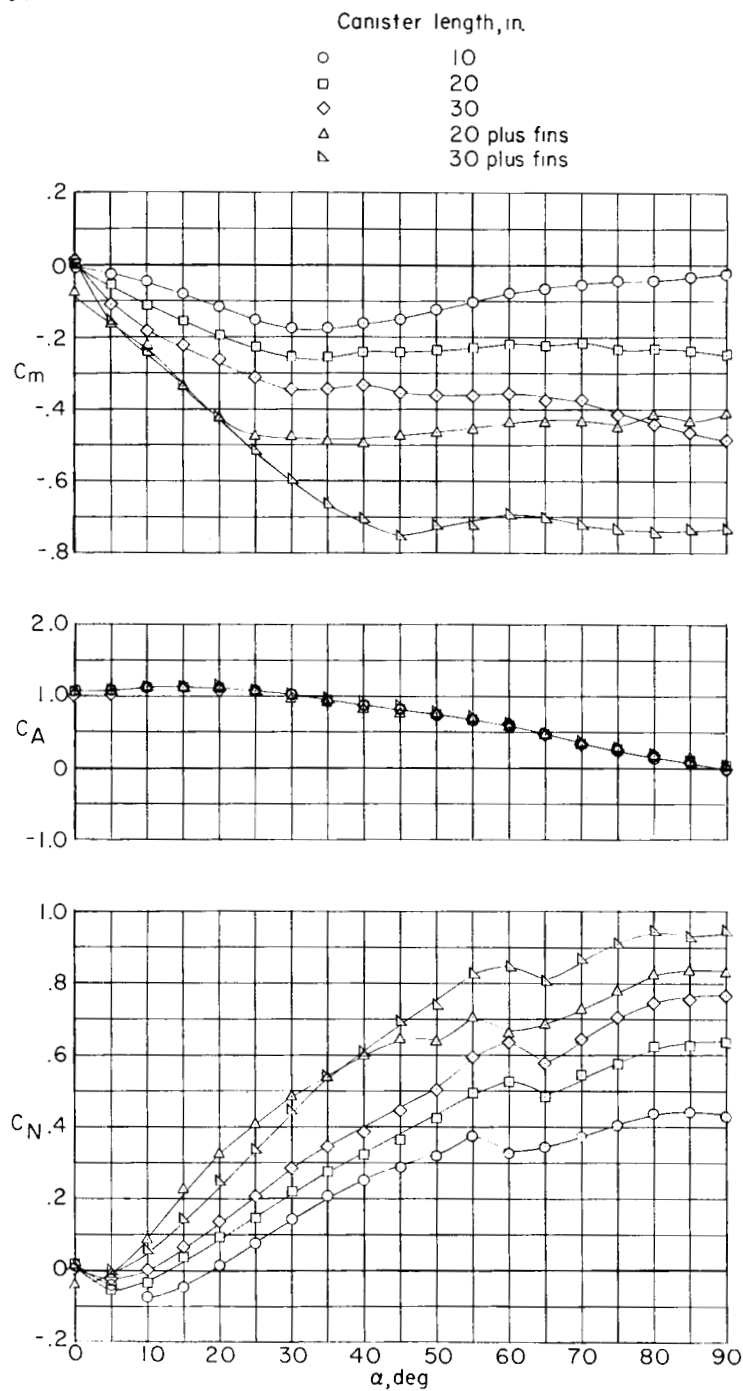
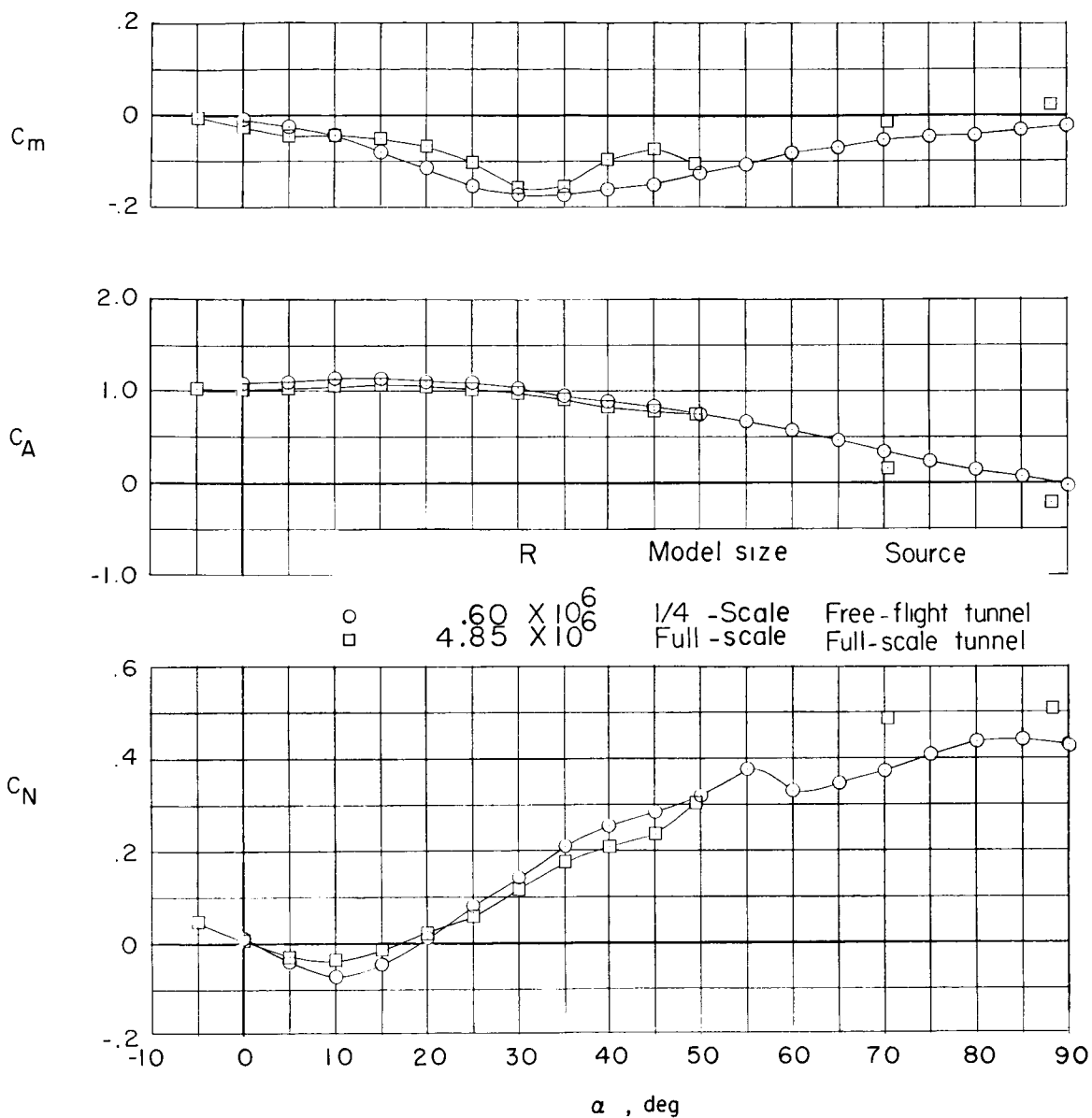


Figure 8.- Effect of extended canister length and the addition of canister fins on the static longitudinal characteristics of the NASA capsule model in the reentry configuration.

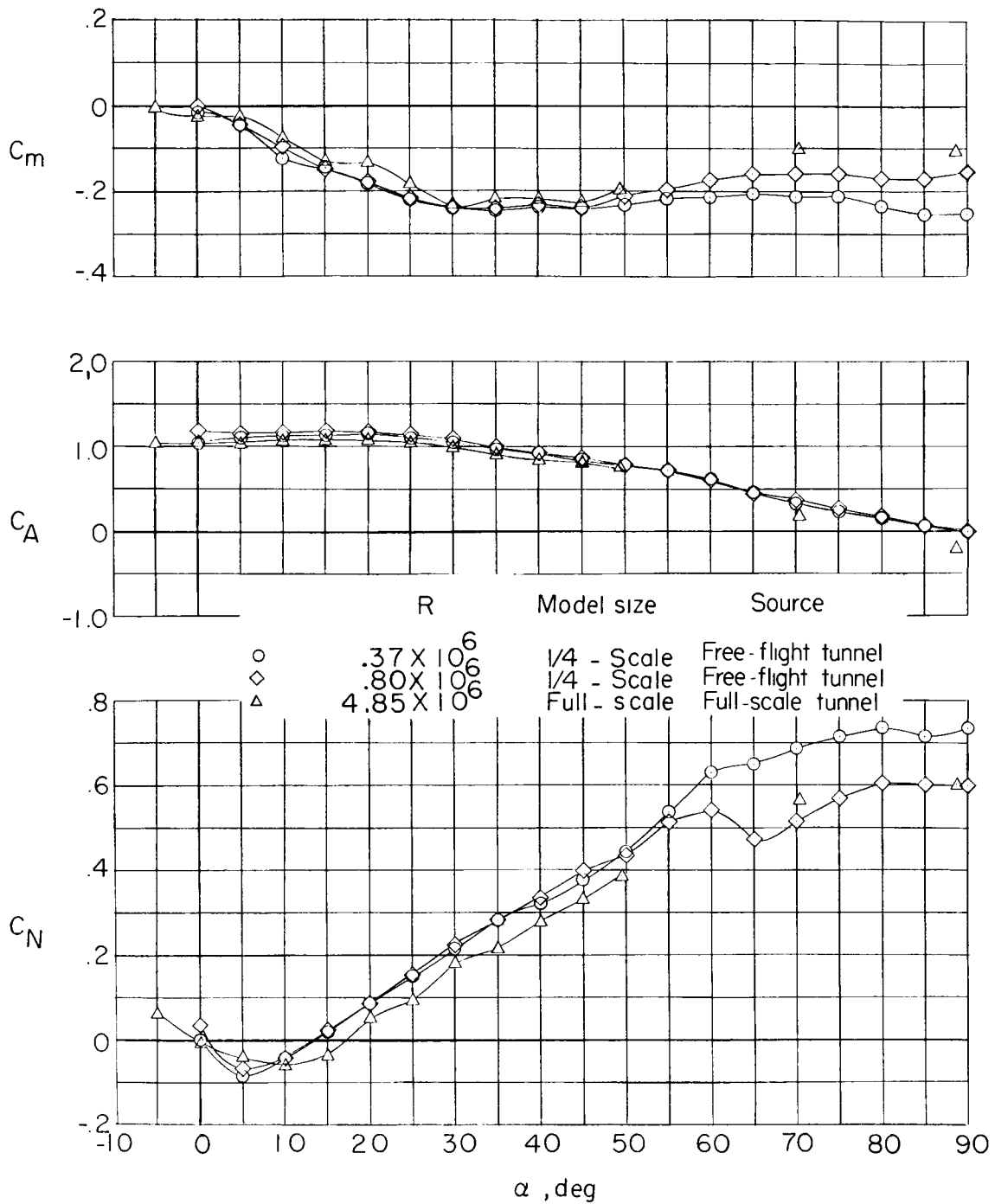
RECEIVED



(a) 10-inch canister.

Figure 9.- Effect of Reynolds number on the low-speed static longitudinal characteristics of models of the NASA capsule in the reentry configuration.

0317: [REDACTED] 30



(b) 17.5-inch canister.

Figure 9.- Concluded.

[REDACTED]

CONFIDENTIAL

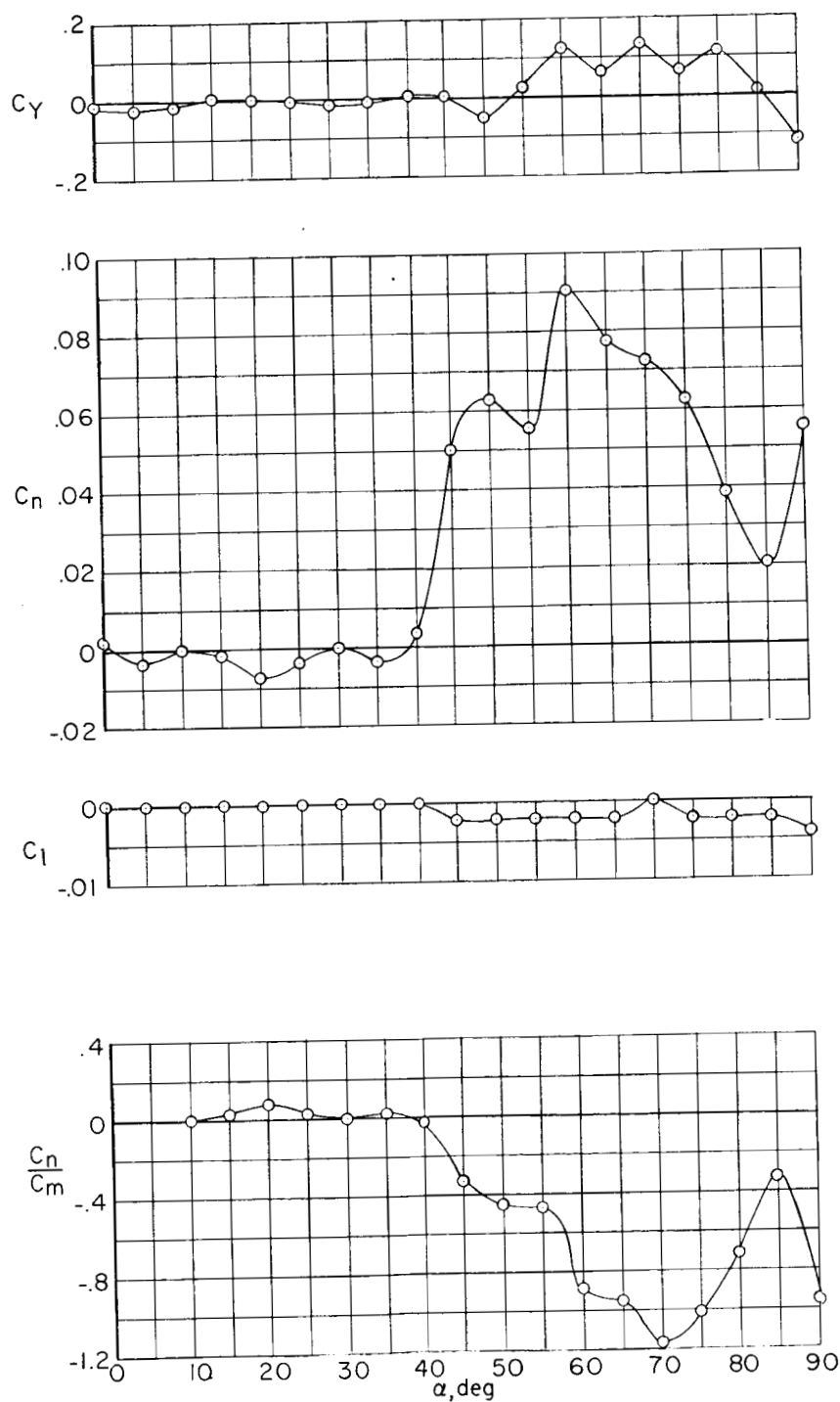


Figure 10.- Lateral stability coefficients at 0° sideslip of the McDonnell capsule model in the reentry configuration.

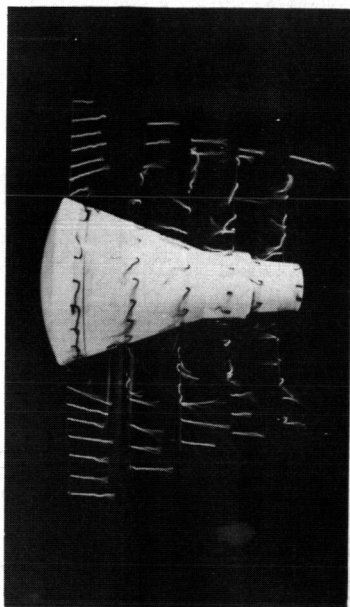
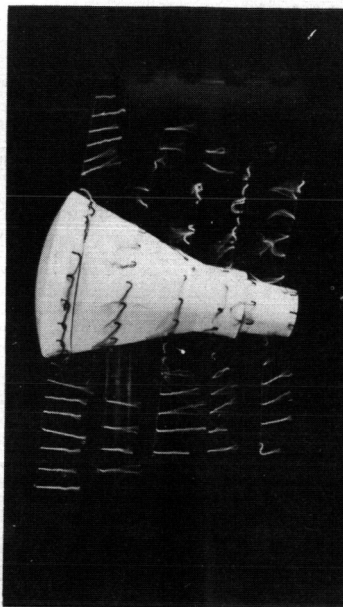
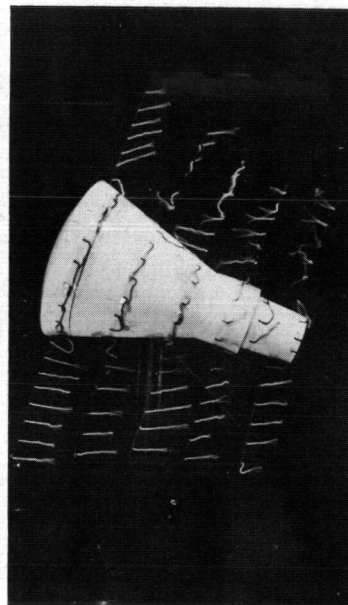
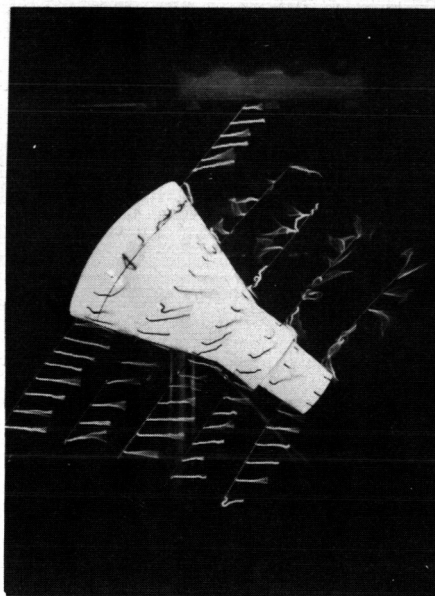
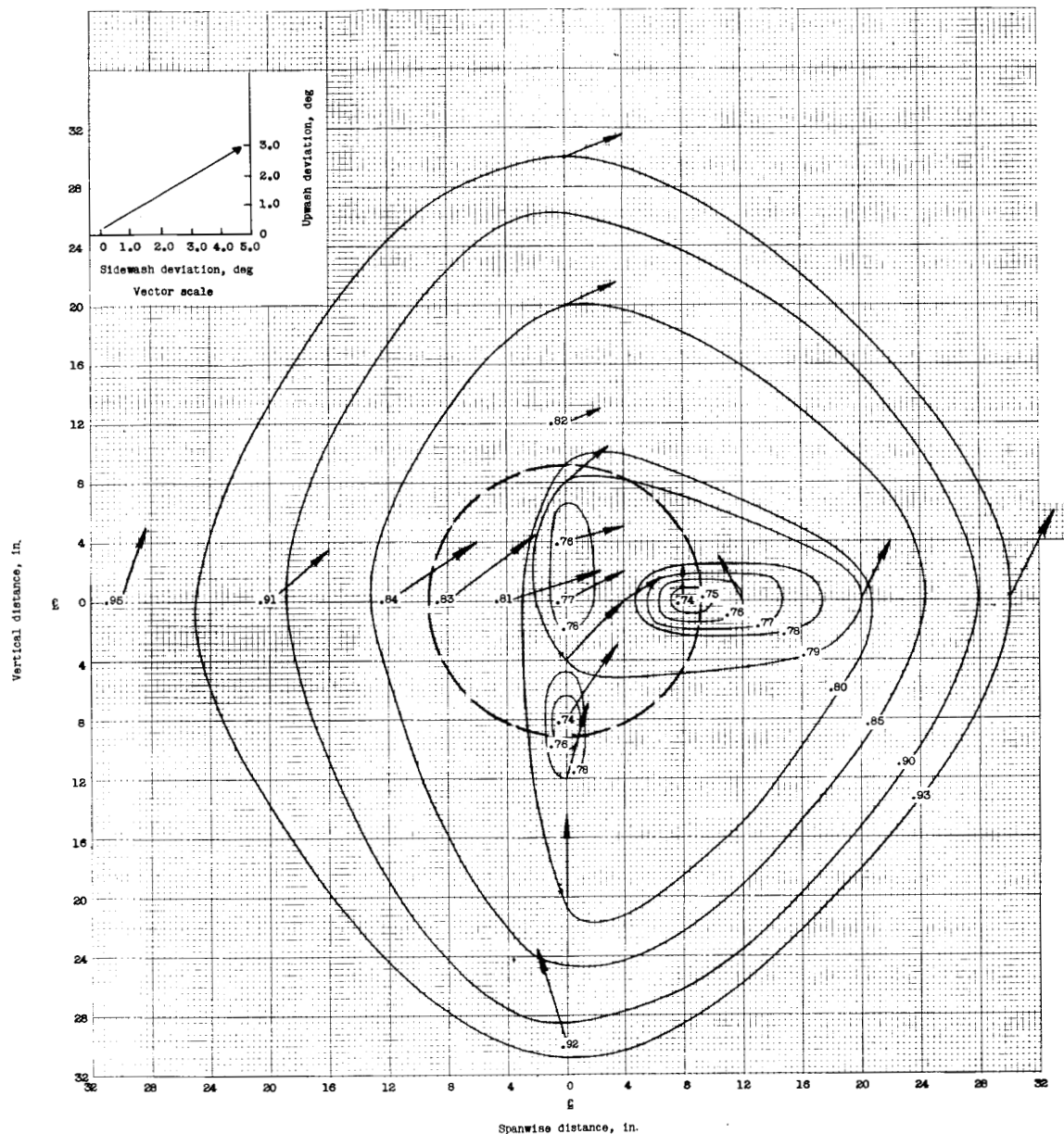
~~CONFIDENTIAL~~ $\alpha = 0^\circ$  $\alpha = 10^\circ$  $\alpha = 20^\circ$  $\alpha = 30^\circ$  $\alpha = 40^\circ$

Figure 11.- Photographs of tuft flow studies of the McDonnell capsule model in the reentry configuration. $\beta = 0^\circ$.

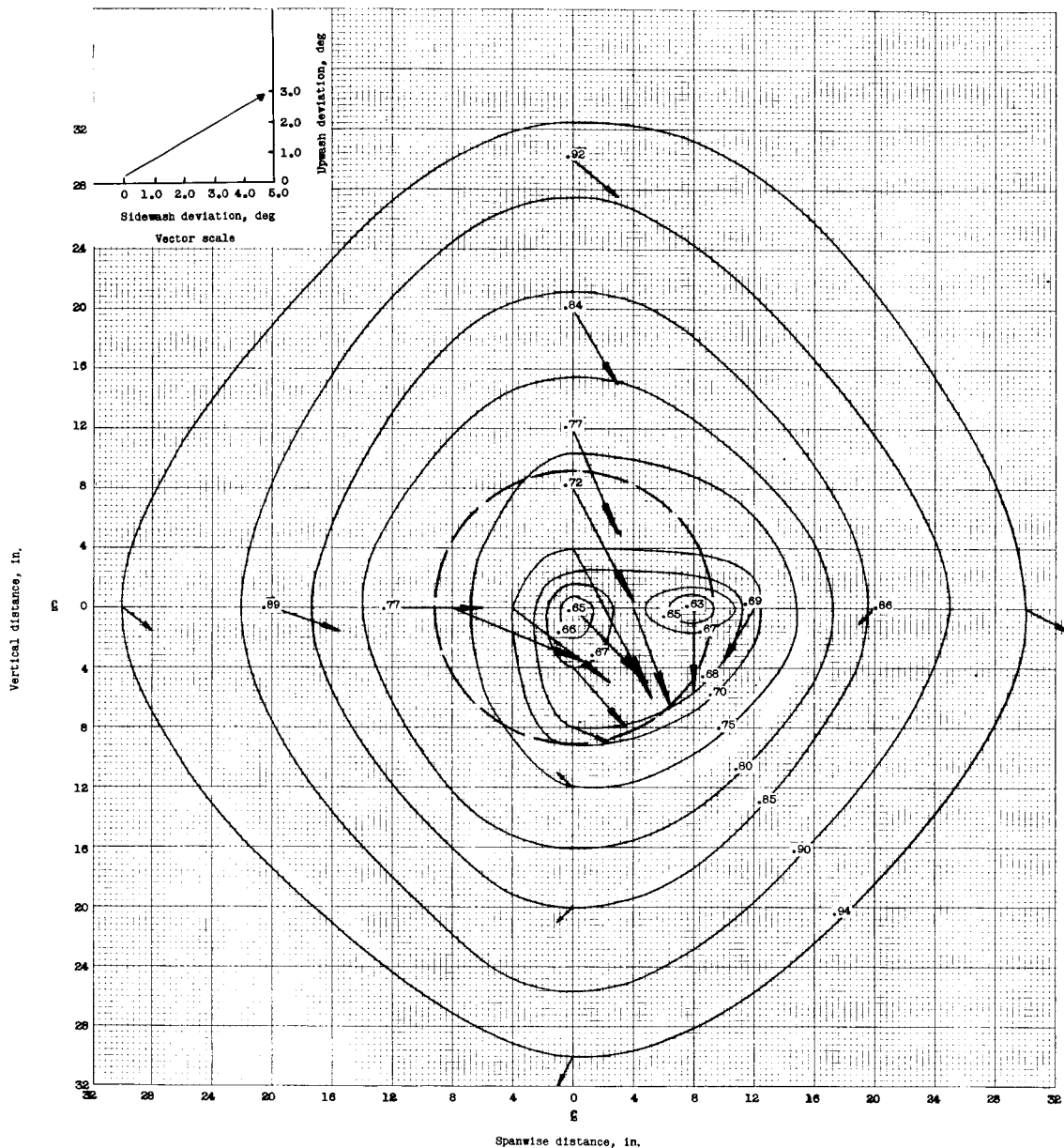
L-60-261

~~CONFIDENTIAL~~



(a) 9 diameters back of reentry configuration.

Figure 12.- Downwash and sidewash angles (vectors denote deviations of air flow from free-stream direction in degrees) and contours of dynamic-pressure ratio, q/q_∞ for the McDonnell capsule model measured in the Langley full-scale tunnel. $\alpha = 0^\circ$, $\beta = 0^\circ$.



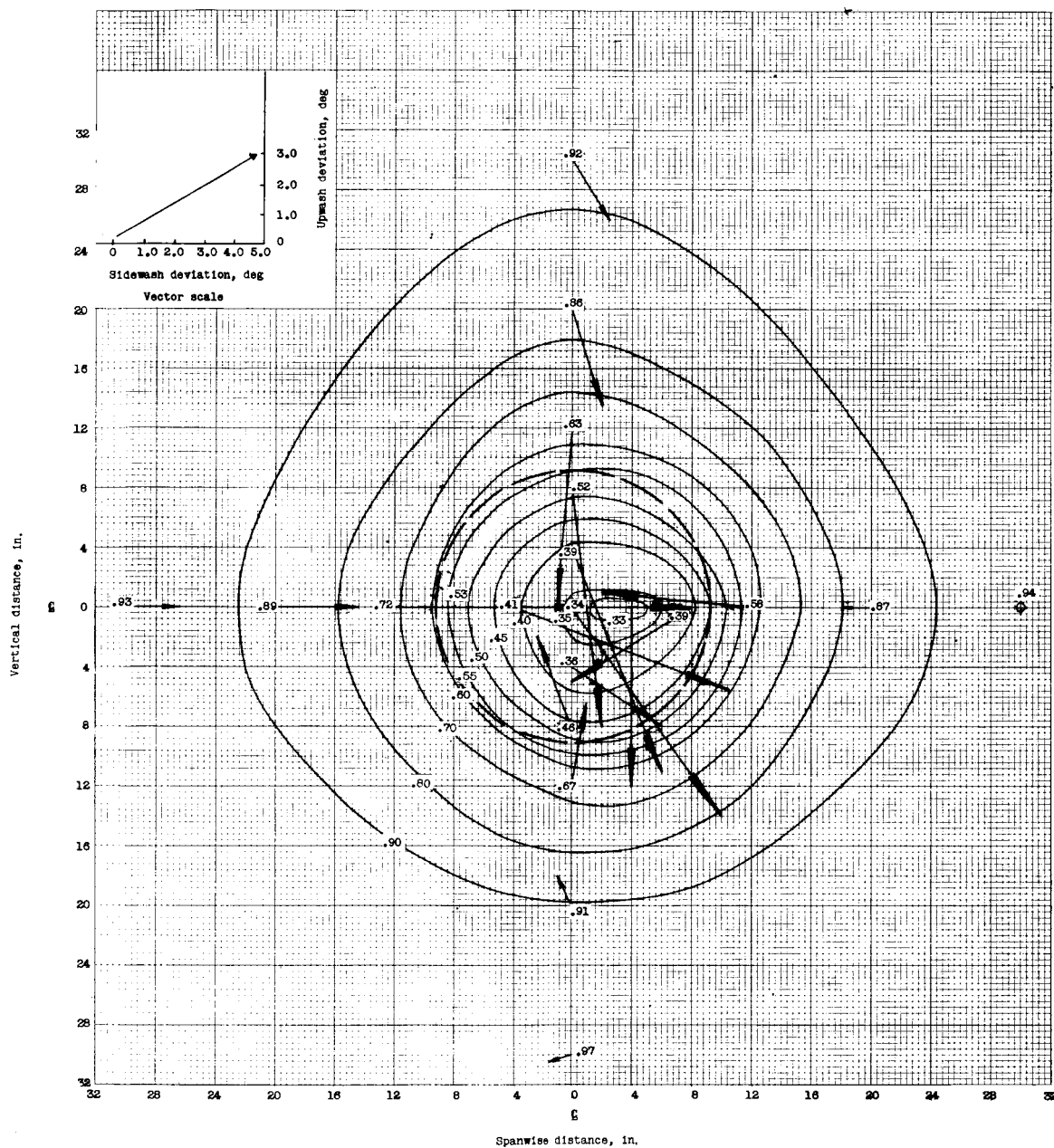
(b) 6 diameters back of reentry configuration.

Figure 12.- Continued.

DECLASSIFIED

35

L-907



(c) 3 diameters back of reentry configuration.

Figure 12.- Concluded.

DECLASSIFIED

03715 [REDACTED] 30

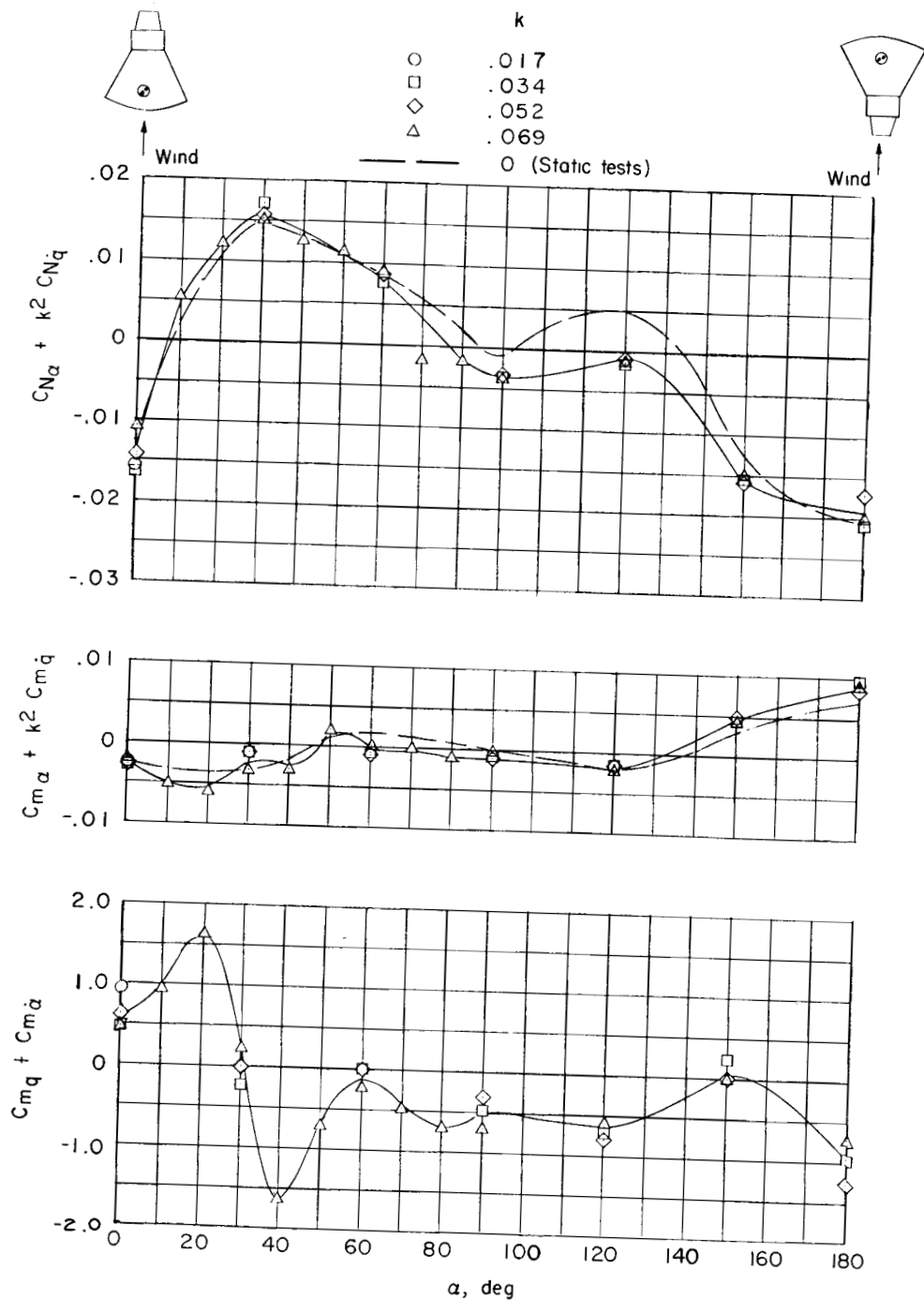


Figure 13.- Longitudinal oscillatory stability derivatives measured in forced oscillation tests in pitch of the McDonnell capsule model in the reentry and exit configurations.

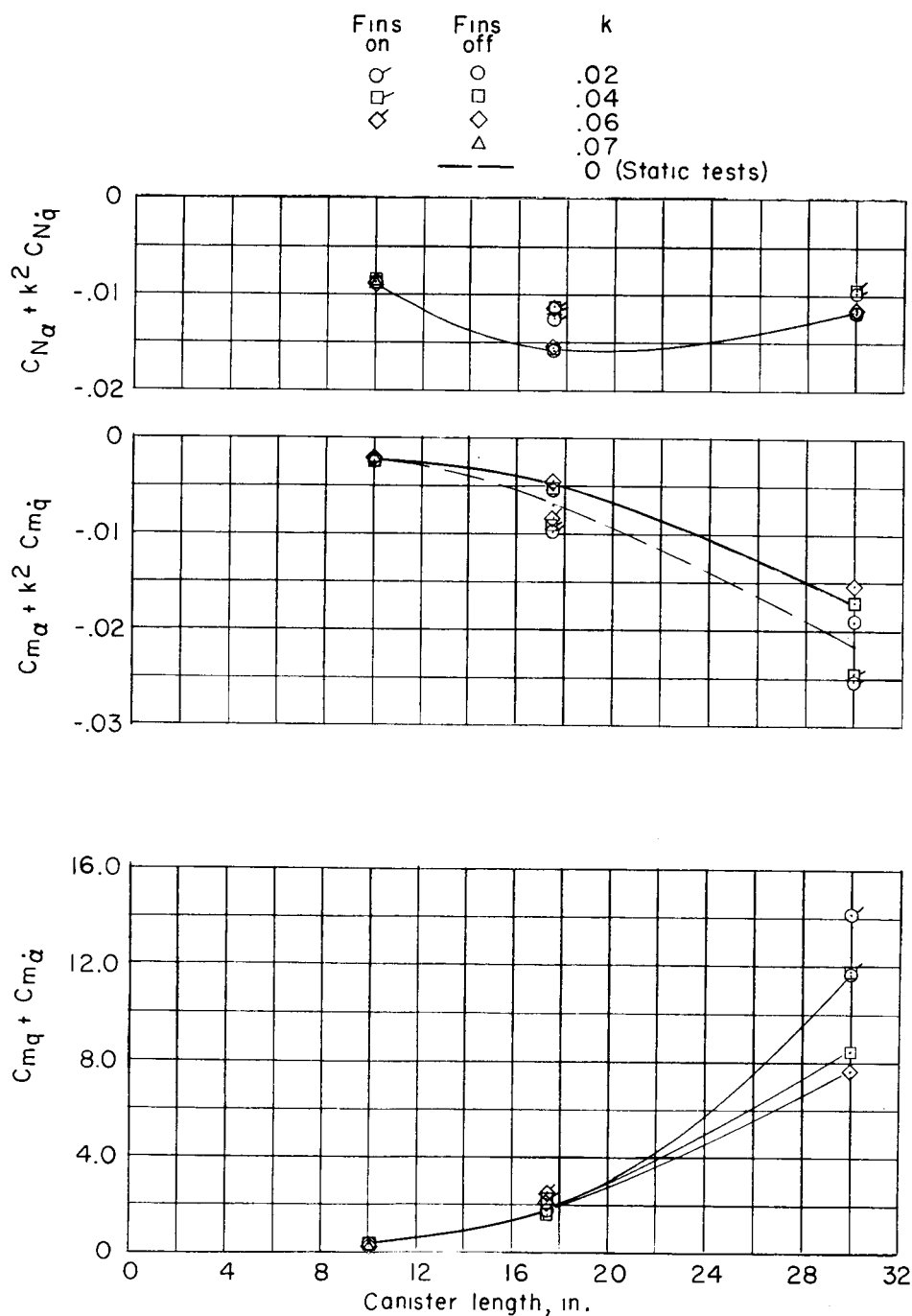


Figure 14.- Longitudinal oscillatory stability derivatives measured in forced oscillation tests in pitch of the NASA capsule model in the reentry configuration. $\alpha = 0^\circ$.

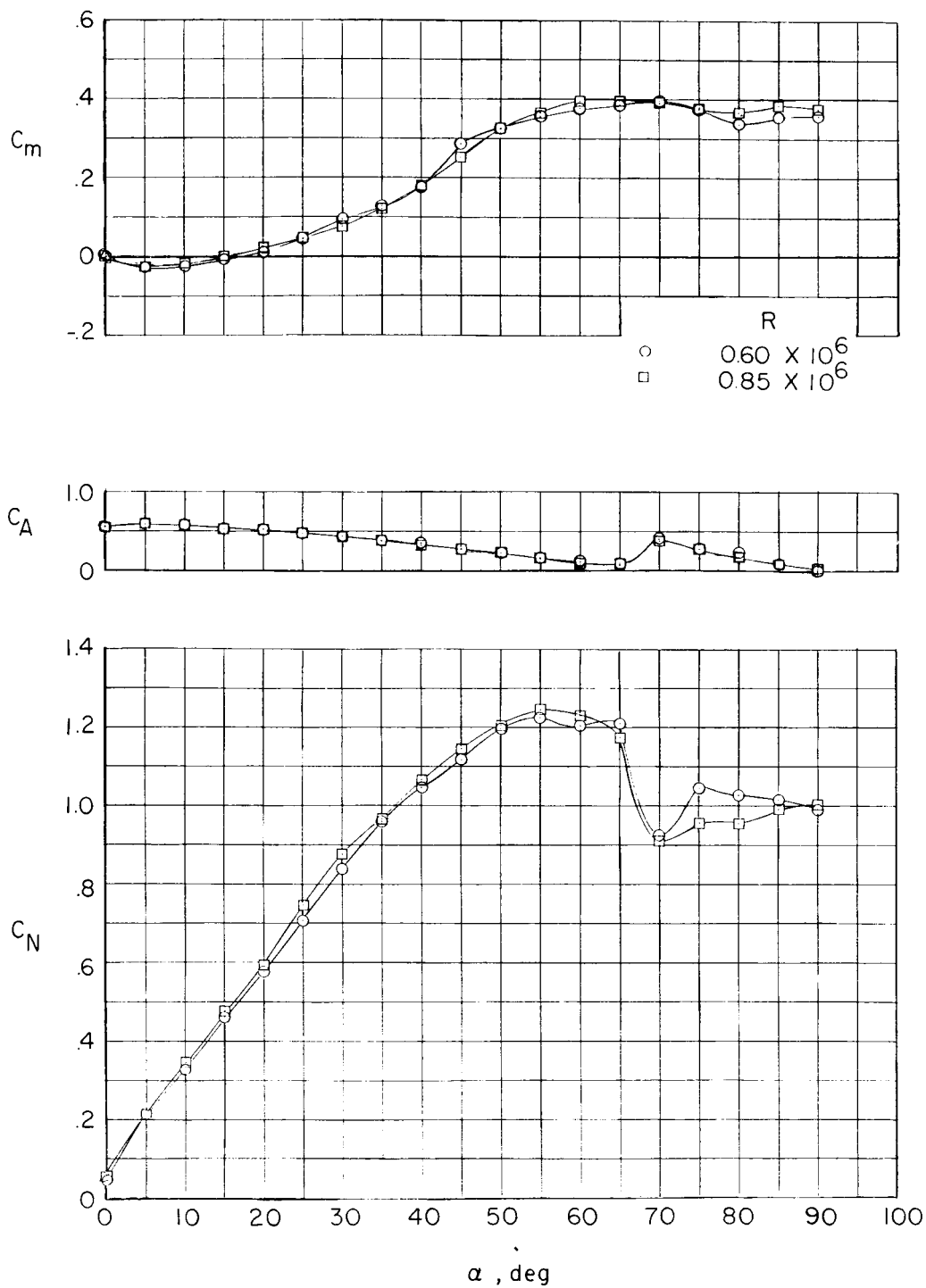


Figure 15.- Static longitudinal characteristics of the McDonnell capsule model in the escape configuration.

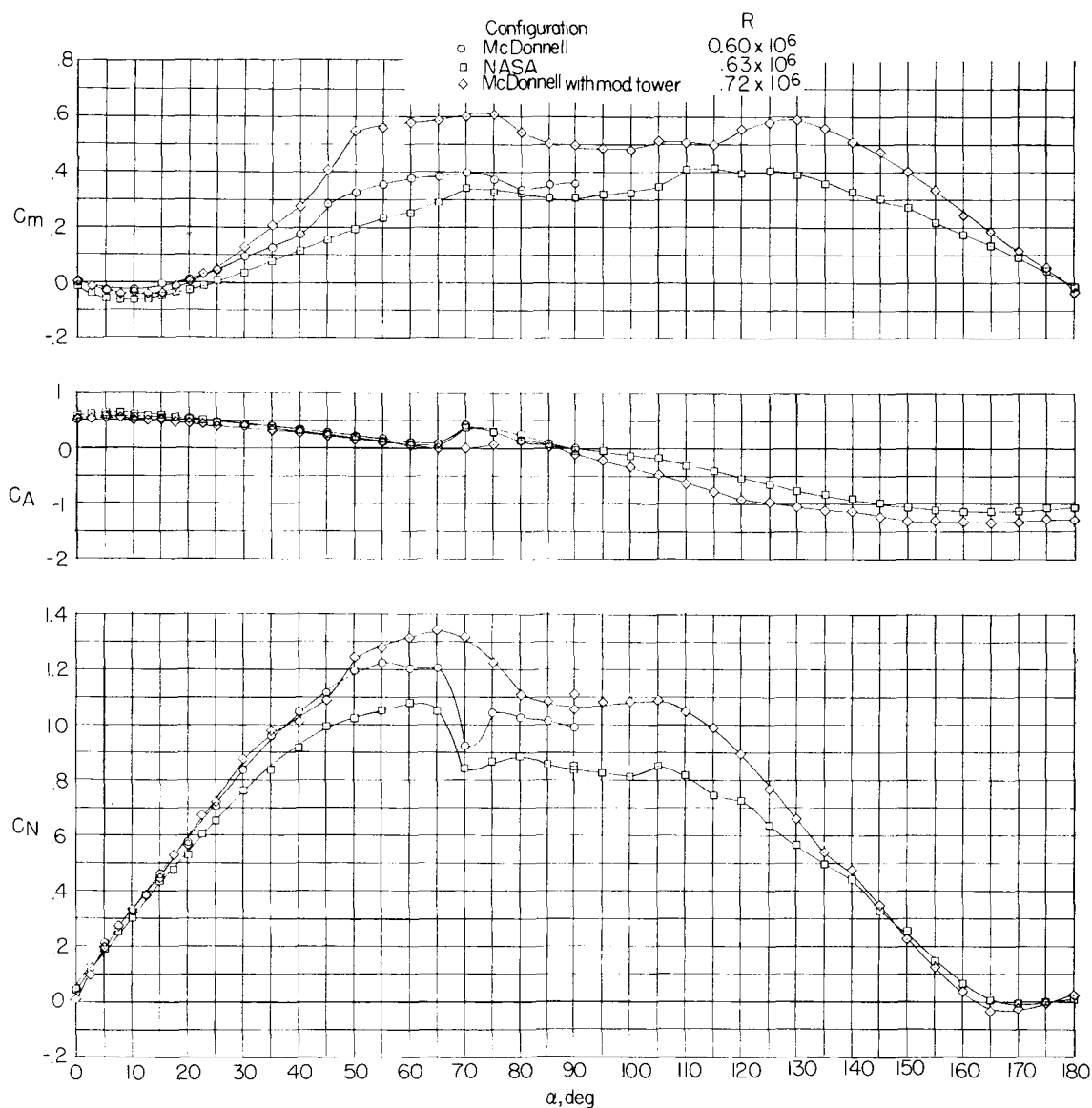


Figure 16.- Comparison of the static longitudinal characteristics of models of several escape configurations.

0371230 1030

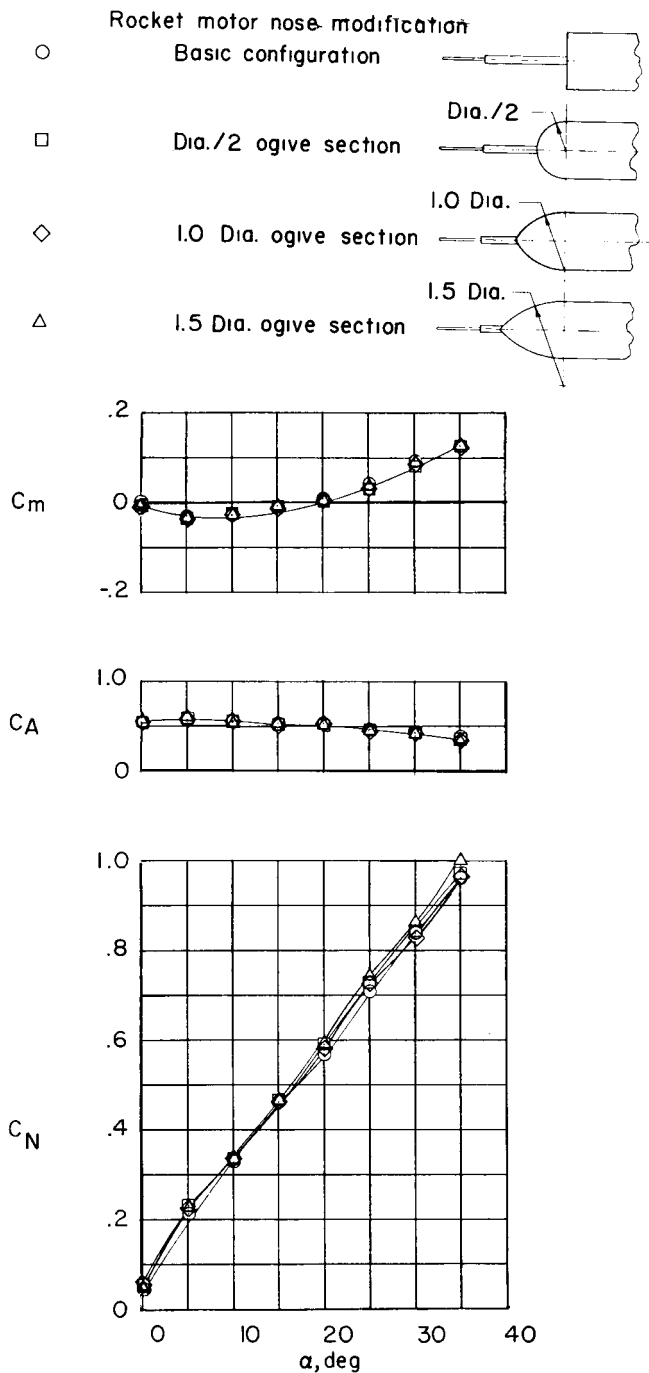


Figure 17.- Effects of modifications to the rocket motor nose section on the static longitudinal characteristics of the McDonnell capsule model in the escape configuration.

DELETED

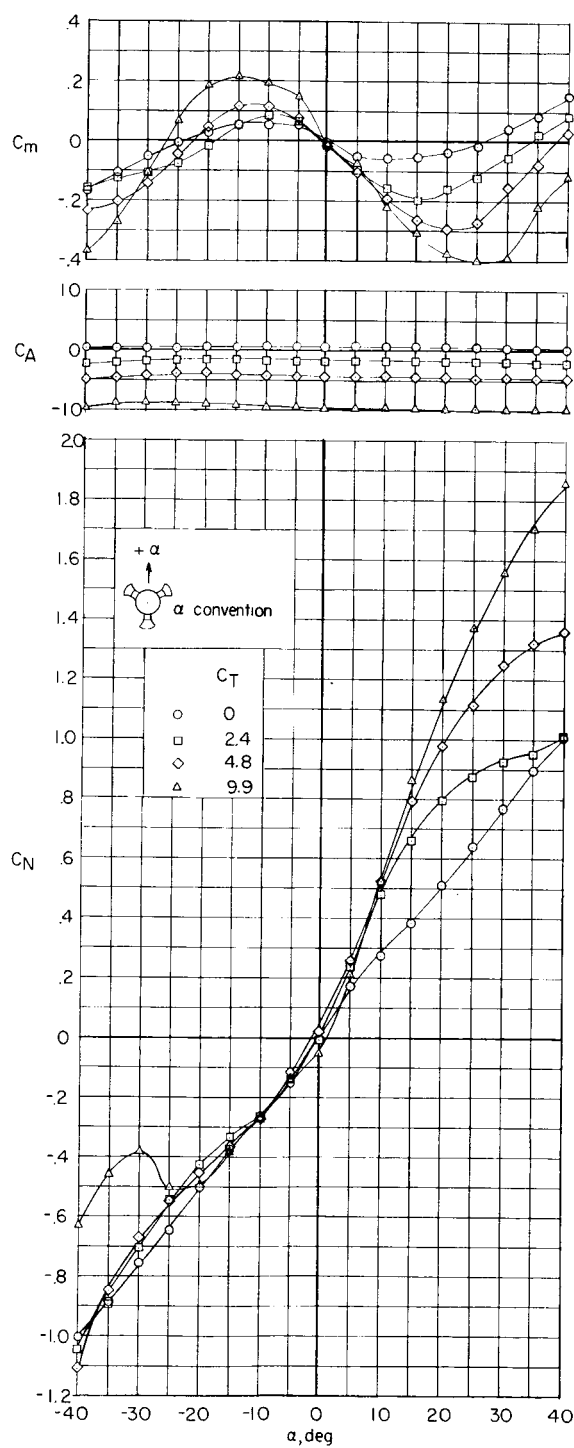


Figure 18.- Power-on static longitudinal characteristics of the model of the NASA capsule in the escape configuration.

03 17 10 20 30

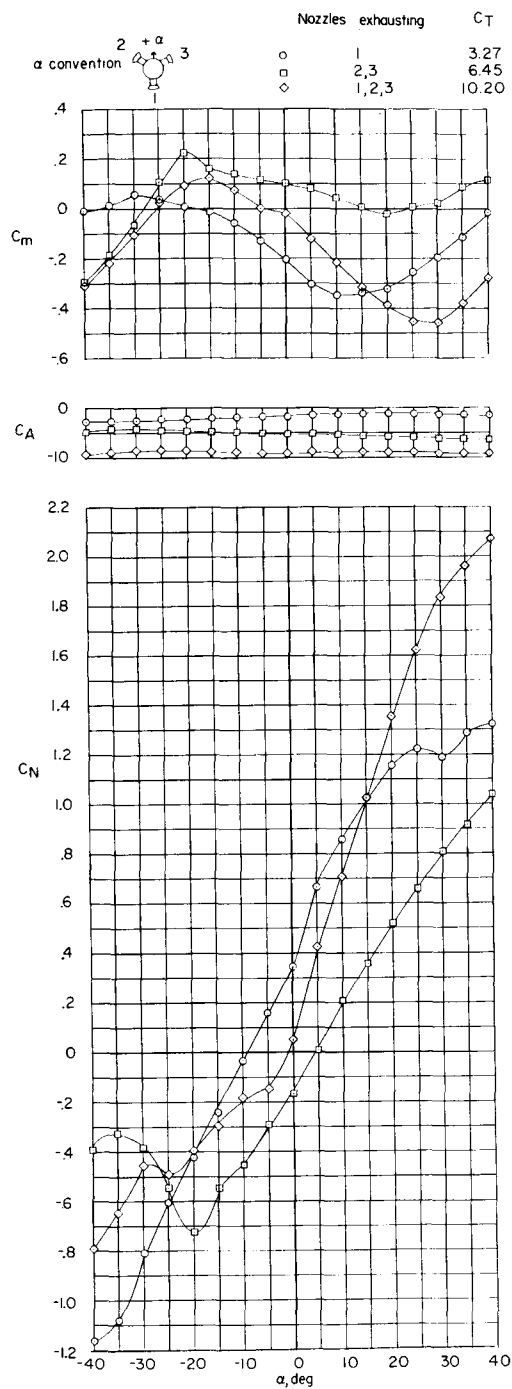


Figure 19.- Effect of thrust asymmetry on the static longitudinal characteristics of the model of the NASA capsule in the escape configuration.

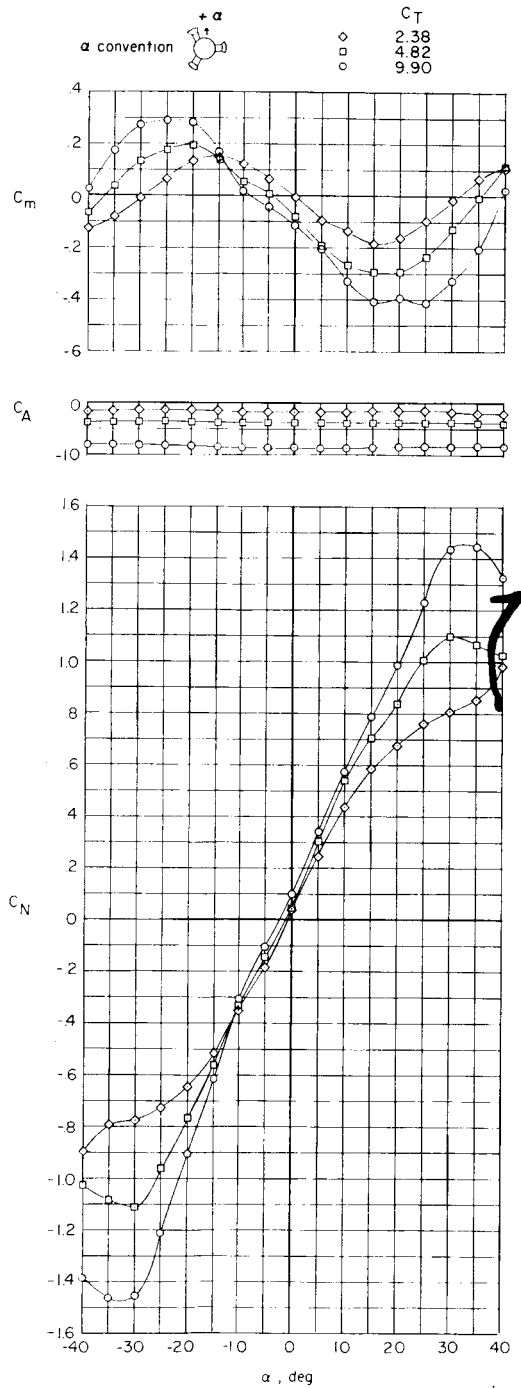


Figure 20.- Static longitudinal characteristics of the NASA capsule model in the escape configuration. (α convention in a plane 90° to that used in figs. 18 and 19.)

03 7 1 2 3 4 5 6 7 8 9 0 3 0

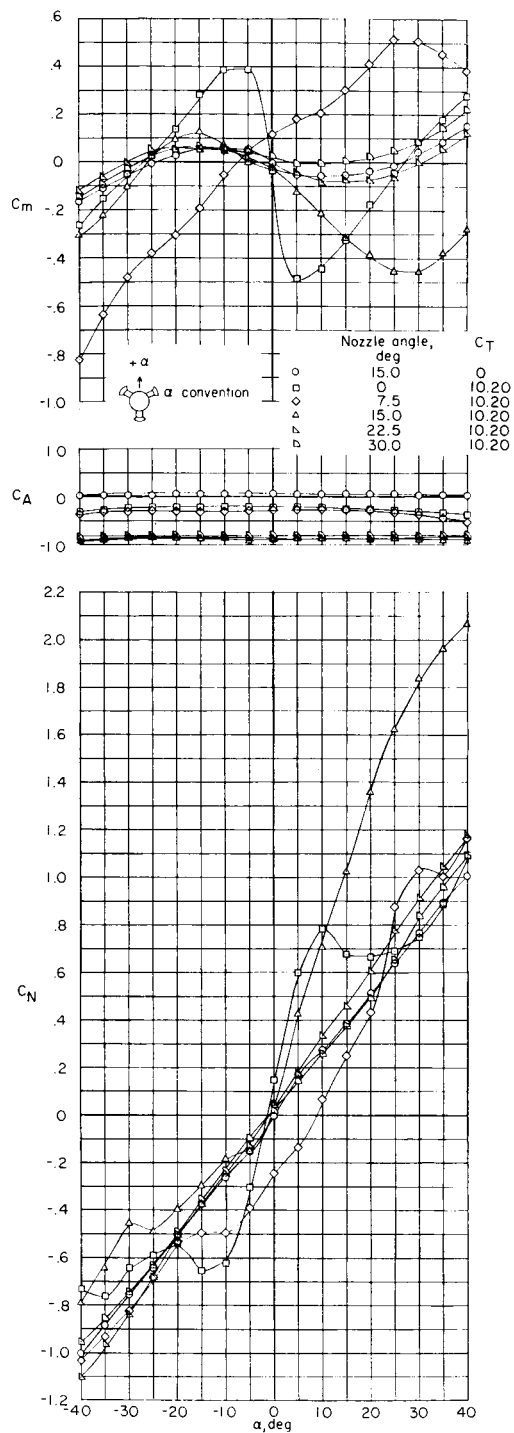


Figure 21.- Effect of nozzle angle on the static longitudinal characteristics of the NASA capsule model in the escape configuration.

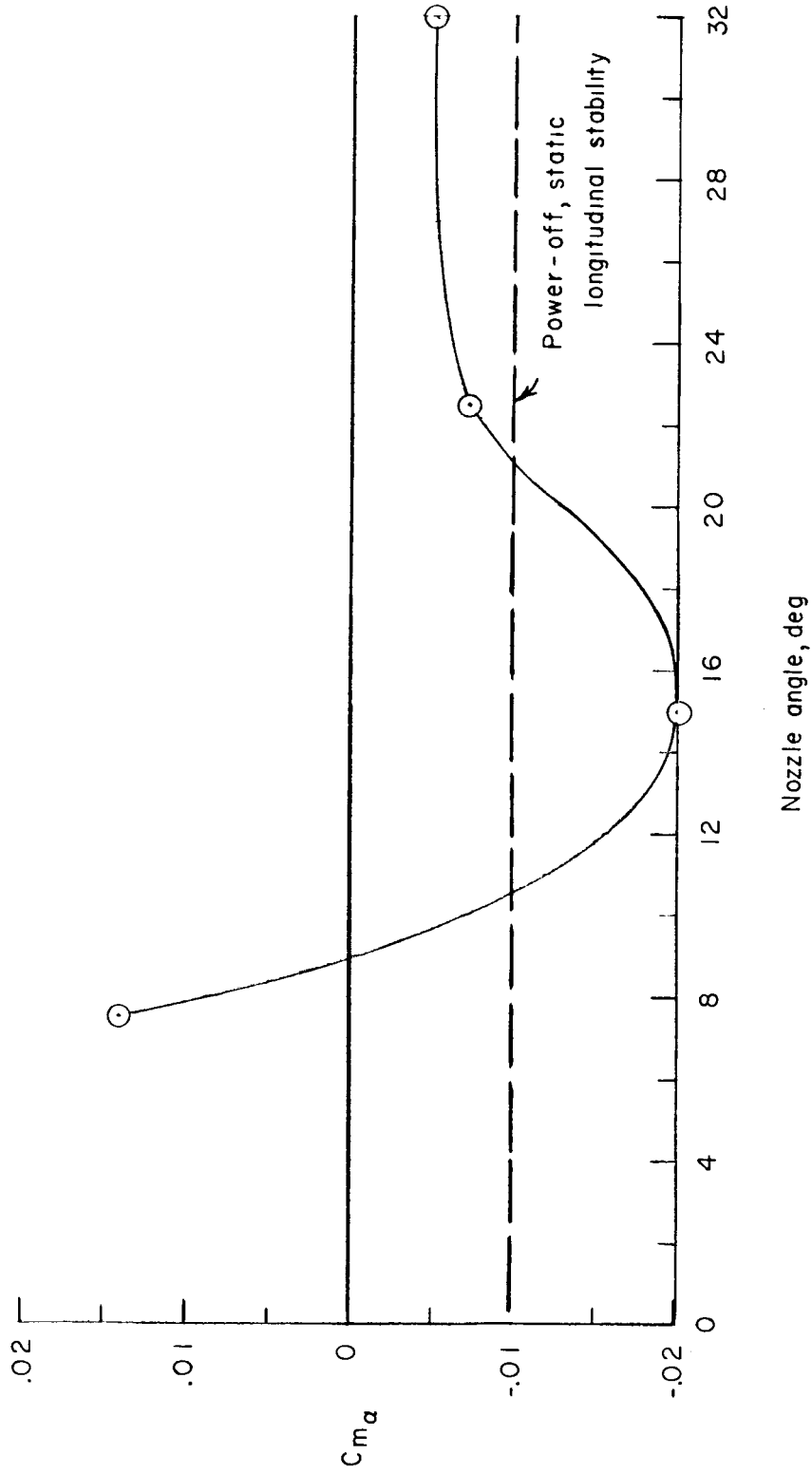


Figure 22.- Variation of the static longitudinal stability parameter C_{m_α} with nozzle angle.
(Data taken from fig. 21 at angles of attack of $\pm 5^\circ$.)

03:70:20:030

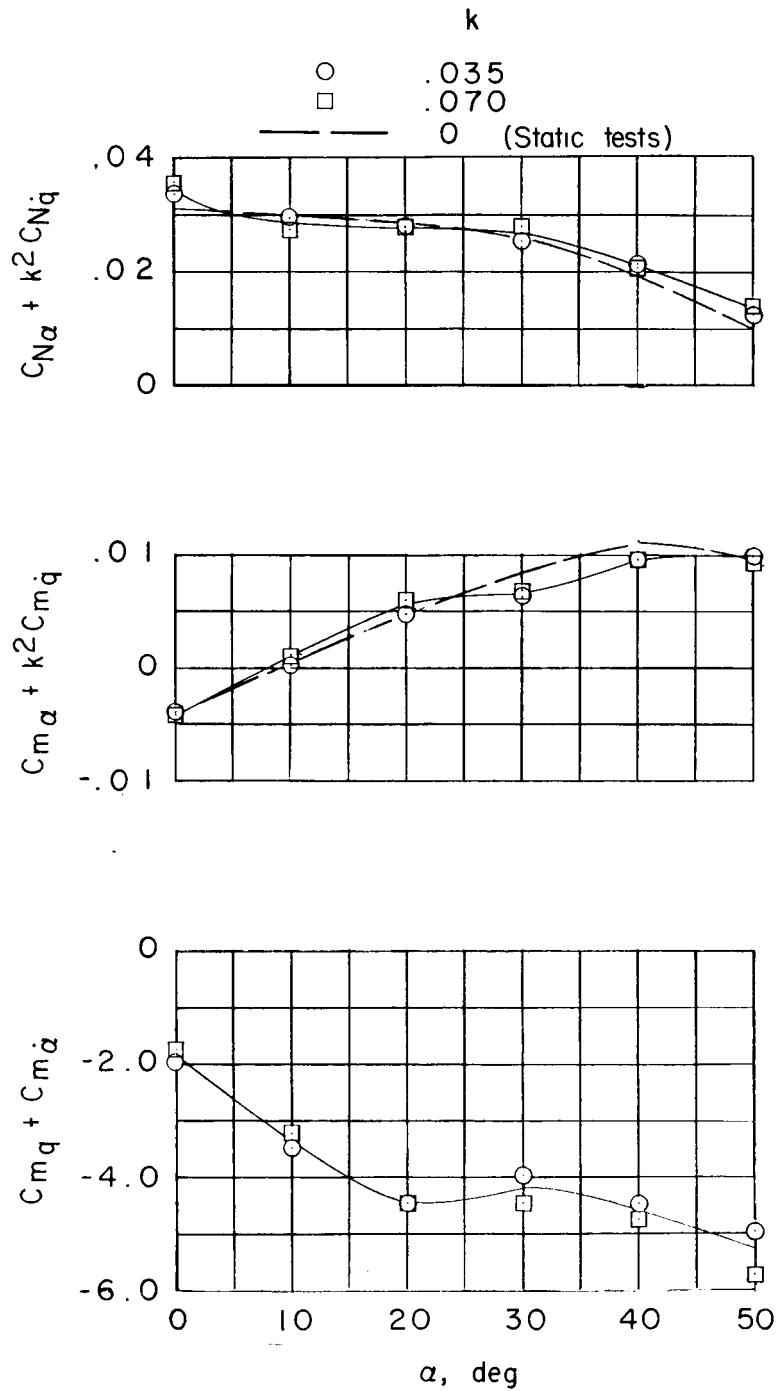


Figure 23.- Pitching oscillation stability derivatives measured in forced oscillation tests in pitch of the McDonnell capsule model in the escape configuration.

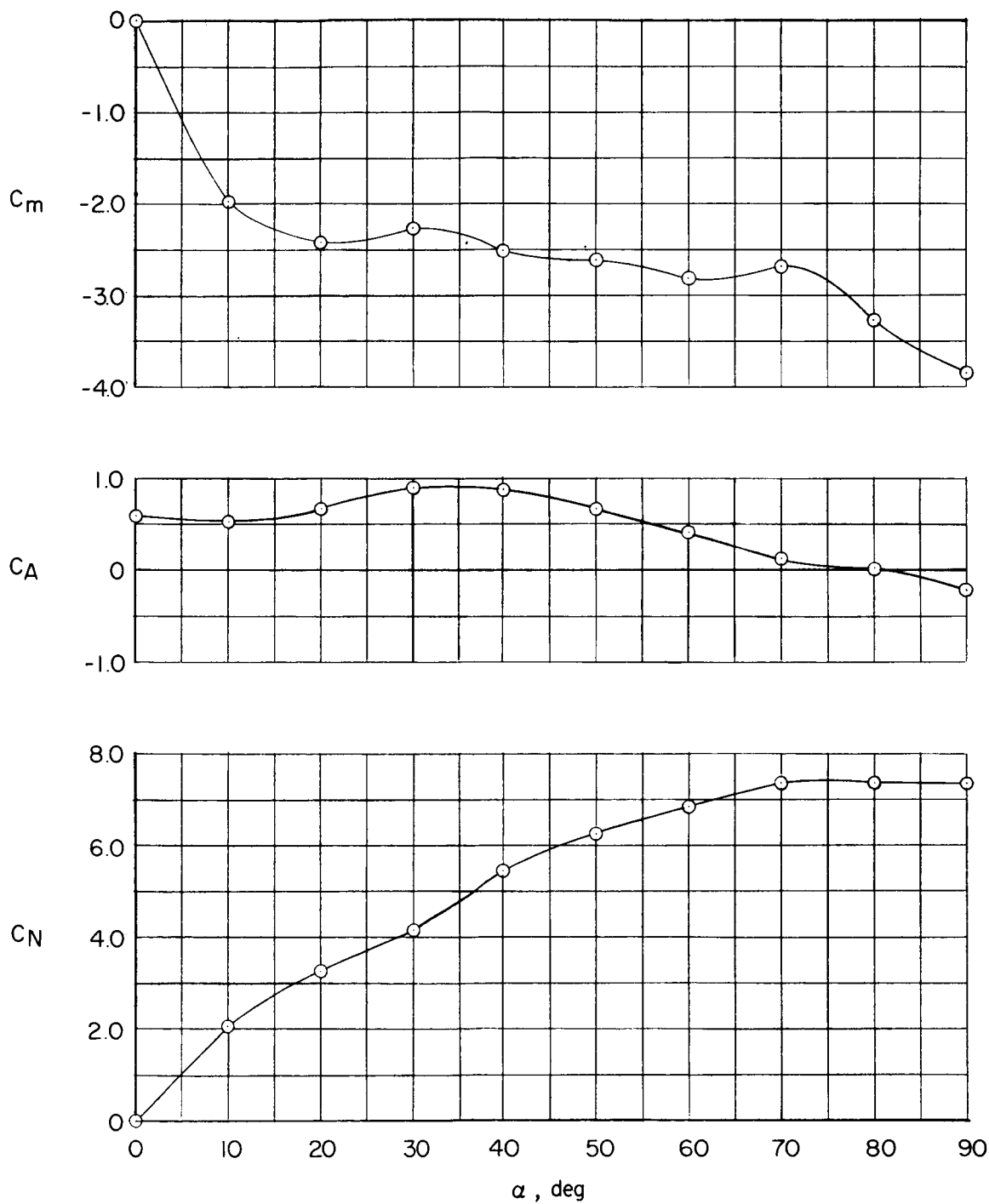


Figure 24.- Static longitudinal characteristics of the Little Joe booster-capsule model.

03 7 1 2 4 10 30

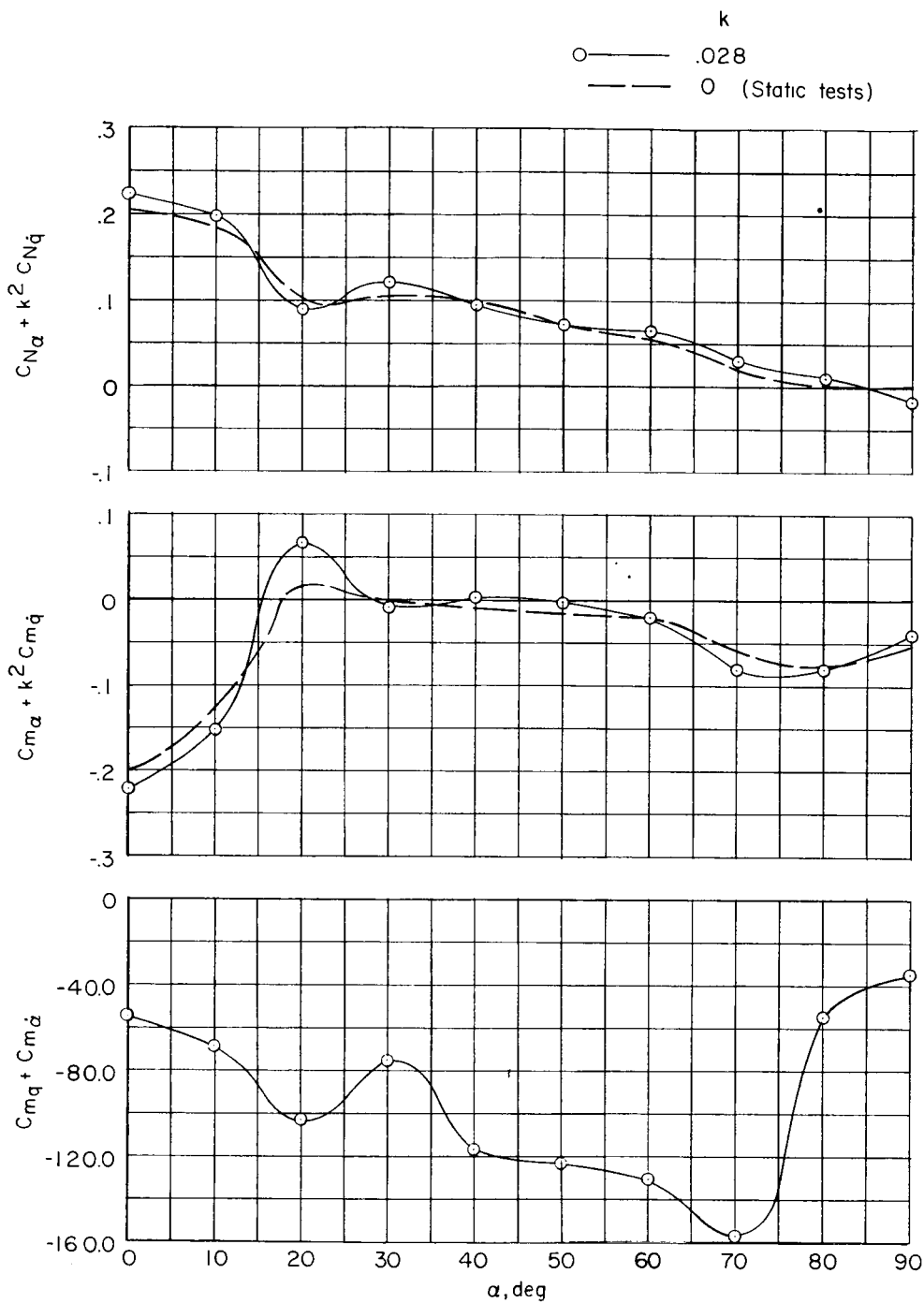


Figure 25.- Pitching oscillation stability derivatives measured in forced oscillation tests in pitch of the Little Joe booster-capsule model.